Pergamon

Geochimica et Cosmochimica Acta, Vol. 68, No. 20, pp. 4039–4058, 2004

0016-7037/04 $30.00 + .00

doi:10.1016/j.gca.2004.01.011

Study of diatoms/aqueous solution interface. I. Acid-base equilibria and spectroscopic observation of freshwater and marine species

A. Gélabert,[1] O. S. Pokrovsky,[1,*] J. Schott,[1] A. Boudou,[2] A. Feurtet-Mazel,[2] J. Mielczarski,[3] E. Mielczarski,[3] N. Mesmer-Dudons,[2] and O. Spalla[4]

[1]Géochimie: Transferts et Mécanismes, UMR 5563, CNRS-OMP-Université Paul Sabatier, 14, Avenue Edouard Belin, 31400 Toulouse, France
[2]LEESA, UMR CNRS 5805, Université de Bordeaux 1, Place du Dr Peyneau, 33120 Arcachon, France
[3]LEM, UMR 7569 CNRS, INPL-ENSG, B.P. 40, 54501, Vandoeuvre-les-Nancy, France
[4]CEA DRECAM/SCM/Groupe Chimie de la Matière Ultradivisée 91191 Gif sur Yvette, France

(*Received August* 1, 2003; *accepted in revised form January* 13, 2004)

Abstract—This work reports on a concerted study of diatom-water interfaces for two marine planktonic (*Thalassiosira weissflogii*= TW, *Skeletonema costatum*= SC) and two freshwater periphytic species (*Achnanthidium minutissimum*= AMIN, *Navicula minima*= NMIN). Proton surface adsorption was measured at 25°C, pH of 3 to 11 and ionic strength of 0.001 to 1.0 M via potentiometric titration using a limited residence time reactor. Electrophoretic mobility of living cells and their frustules was measured as a function of pH and ionic strength. Information on the chemical composition and molecular structure of diatoms surfaces was obtained using FT-IR (in situ attenuated total reflectance) and X-ray Photoelectron Spectroscopy (XPS). The surface area of living cells and their frustules in aqueous solutions was quantified using Small Angle X-ray Scattering Spectroscopy (SAXS).

These observations allowed us to identify the nature and to determine the concentration of the major surface functional groups (carboxyl, amine and silanol) responsible for the amphoteric behavior of cell surfaces in aqueous solutions. Taking into account the relative proportion of surface sites inferred from XPS and FT-IR measurements, a surface complexation model of diatom-solution interfaces was generated on the basis of surface titration results. The cell-normalized ratios of the three major surface sites {>COOH}: {>NH_3}: {>SiOH} are 1:1:0.1, 1:10:0, 1:1:0.4 and 1:1:0.3 for TW, SC, AMIN and NMIN, respectively. The total amount of proton/hydroxyl active surface sites for investigated species ranges from 1 (NMIN) to 9 (SC) mmol/g dry weight. Normalization of these site densities to the area of siliceous skeleton yields values between 0.3 (NMIN) and 0.9 mmol/m^2 (SC) which are an order of magnitude higher than corresponding values for organic-free frustules or amorphous silica. This suggests that the amphoteric properties and possibly the affinity for metal adsorption of diatom cultures are essentially controlled by the 3-D organic layers covering the silica frustule. *Copyright © 2004 Elsevier Ltd*

1. INTRODUCTION

Diatoms, unicellular photosynthetic algae enclosed in an external siliceous skeleton called frustule, are largely widespread in marine and freshwater environments. They constitute an important organic carbon reservoir providing more than a quarter of the primary production on the earth. Diatoms are known to exhibit a strong affinity for a wide range of dissolved trace elements. As a result, they exert a strong control on the transfer of heavy metals along the water column up to the sediments, thereby regulating the concentration of dissolved metal ions. This binding capacity of the diatom surfaces and their frustules can also be used for various technological applications, for example, to remove toxic metals from polluted environments (Volesky and Holan, 1995; Csogor et al., 1999; Vrieling et al., 1999; Schmitt et al., 2001). From an ecotoxicological point of view, diatoms being at the beginning of the trophic chains, they play a major role in heavy metals (i.e., Zn, Cd) bioaccumulation and bioamplification along the food webs. Various diatom species are also used for detection of changes in water quality due to their specific sensitivity to metal pollution (Gold et al., 2002, 2003). Numerous studies have been devoted to metal uptake by diatoms (Fisher, 1986; Fisher and Reinfelder, 1995; Sunda and Huntsman, 1998), excretion of ligands in response to metal stress (Fisher and Fabris, 1982; Zhou and Wangersky, 1989; Morel et al., 1994; Ahner et al., 1997; Pistocchi et al., 2000), and diatom growth limitation by trace elements (Anderson et al., 1978; Brand et al., 1986; Morel et al., 1991; Sunda and Huntsman, 1995, 1998). Since biosorption involves a set of both active and passive transport mechanisms whose first step is the interaction of the metal ion with the cell wall, the surface of the cells is likely to play a predominant role in the binding of heavy metals. However, rigorous understanding and modeling of the interactions between trace elements and diatoms surfaces are still lacking which prevents to quantitatively assess the role diatoms play in the regulation of metal transport in surficial aquatic environments. This study is a part of concerted efforts initiated by our group and aimed at the thermodynamic characterization of diatoms/aqueous solution interfaces.

Diatom frustule is covered by an organic coat, composed of organic molecules such as polysaccharides, amino acids and glycoproteins, tightly associated with silica (Kates and Volcani, 1968; Hecky et al., 1973; Swift and Wheeler, 1992; Kroger et al., 1994). The numerous functional groups present on the surface of cell walls can be proton active within the acidity range of natural waters and their protonation/deprotonation is

* Author to whom correspondence should be addressed (oleg@lmtg.obs-mip.fr).

Table 1. Physical characteristics of diatom cultures.

Species	Shape and size	Weight of humid diatoms (g/cell)	Weight of lyophilized diatoms (g/cell)	Weight of dry frustules (g/cell)	BET N_2 surface of dry frustules (m^2/g)	SAXS surface of dry frustules (m^2/g)	SAXS surface of viable cells (m^2/cell)
AMIN	Pennate, 12 × 4 μm	3.7×10^{-9}	2.1×10^{-10}	1.0×10^{-10}	12.8	13	$\geq 6.0 \times 10^{-10}$
NMIN	Pennate, 7 × 3 μm	1.0×10^{-8}	9.95×10^{-10}	4.3×10^{-10}	7.7	6	$\geq 4.0 \times 10^{-10}$
TW	Centric, 10 μm	1.8×10^{-8}	1.4×10^{-9}	3.6×10^{-11}	74.3	44	2.4×10^{-9}
SC	Centric, 10 μm	2.3×10^{-9}	3.7×10^{-10}	2.4×10^{-11}	156	67	2.8×10^{-9}

responsible for the amphoteric properties of diatom surfaces in aqueous solution. The goal of this work is the identification of the functional groups present on diatom surfaces and the quantification of their concentrations and protonation/deprotonation constants. For this purpose, we used a multiple experimental approach which combined conventional macroscopic techniques (surface titration, electrophoresis) and surface spectroscopic observations. Over the last decade, significant amount of work has been devoted to the characterization of bacterial and algal surfaces in aqueous solutions via potentiometric titrations (Crist et al., 1981, 1988, 1990, 1992; Plette et al., 1995, 1996; van der Wal et al., 1997b; Daughney and Fein, 1998; He and Tebo, 1998; Martinez et al., 2002), adsorption experiments (Goncalves et al., 1987; Goncalves and Lopez da Conceicao, 1989; Ledin, 2000), electrophoresis (Richmond and Fisher, 1973; Bayer and Sloyer, 1990; Kijlstra and van der Wal, 1995; van der Wal et al., 1997a; Ulberg and Marochko, 1999; Boonaert and Rouxhet, 2000) and spectroscopic observations (Busscher et al., 1990; Naumann et al., 1991; Rouxhet and Genet, 1991; Dufrène et al., 1997; Keifer et al., 1997). These studies allowed comprehensive understanding of the thermodynamic and chemical properties of bacterial surfaces and their affinities for metal ions (Beveridge, 1988; Beveridge et al., 1995, 1997; Fein et al., 1997). In contrast, with the exception of a few studies on marine diatoms (Gonzalez-Davila, 1995; Gonzalez-Davila et al., 1995, 2000), little attention has been devoted until now to the physico-chemical properties of diatoms surfaces. In this study, we retained four representative diatom species, two planktonic, *Skeletonema costatum* (marine) and *Talassiosira weisflogii* (estuarine) and two freshwater peryphytic (i.e., linked to submerged support), *Achnanthidium minutissimum* and *Navicula minima,* to elaborate a thermodynamic model of their surfaces in aqueous solutions and predict metal-diatoms interactions.

MATERIALS AND METHODS

2.1. Culture Processes and Characterization of Diatoms

2.1.1. Diatoms Culture Conditions

Monospecific diatom cultures were developed from laboratory strains to produce biomass of four species: marine planktonic *Thalassiosira weissflogii* (abbreviated TW), *Skeletonema costatum* (SC), freshwater periphytic *Achnanthidium minutissimum* (AMIN) and *Navicula minima* (NMIN). Axenic strains of AMIN and NMIN were obtained from FDCC (Freshwater Diatom Culture Collection), Iowa, U.S.A. Periphytic diatoms were cultured at 20°C in sterile Dauta medium (Dauta, 1982) at pH ~ 7.7 using 2500 mL Erlenmeyer flasks placed in a thermo-regulated chamber under a light intensity of 30 μmol photon m^{-2} s^{-1} on a 14:10-light:dark cycle to concentration of $\sim 10^7$ cell/L. Continuous aeration of the culture was insured to prevent pH from increasing due to photosynthetic activity. The same culture conditions were used for *Thalassiosira weissflogii* and *Skeletonema costatum* given by CREMA (Centre de Recherche en Ecologie Marine et Aquaculture), L'Houmeau, France, but in a standard nutrient medium f/2 (Guillard, 1975) at pH ~ 8.0. Typical incubation time was 2–4 weeks. During diatoms production process, weekly transfers of aliquots of each culture in a new medium allowed us to increase growth speed of each strain and to collect high amounts of biomass. Diatoms were harvested from the stationary growth phase and kept at 4°C until use. Before all experiments described below, algae were rinsed in appropriate (0.001–1 mol/L) NaCl or $NaNO_3$ aqueous solutions.

2.1.2. Physical Characterization and SAXS Measurements

Concentration of diatom cell suspension was quantified by: *1)* cells counting using a Nageotte cell under light microscopy (at least 10 counts of approx. 80–100 cells were performed and the average value with a typical uncertainty of 10–20% was taken); *2)* measurement of the optical density of suspensions using a spectrophotometer at 400 nm wavelength (good linear correlation between the optical density and cell number was obtained in the range 2×10^8–2×10^9 cell/L); *3)* weighing the wet centrifuged pellets (20 min at 2500 g); and *4)* freeze-drying the centrifuged pellets. Diatom frustules were obtained after HNO_3+H_2O_2 digestion of cell biomass during 6 h on a sand bath at 220°C. Specific surface area of frustules was measured by N_2 (3 points) and Kr (multipoint) adsorption using the BET method. Agreement within ±10% between these methods was found. The humid and dry weights of cells and their frustules together with specific surface area of each species are given in Table 1. The size and geometric area of viable cells were assessed from high-resolution environmental SEM and TEM images taken by a Scanning Electron Microscope Philips 515 and a Transmission Electron Microscope Philips CM 10, respectively. Representative images of the diatom species are given in Figure 1. It can be seen from TEM images that the thickness of the organic layer coating silica frustule varies from 100–200 nm for AMIN to 400 ± 100 nm for TW.

Surface fine structure and porosity of diatom frustules and viable cells were estimated via Small Angle X-ray Scattering Spectroscopy (SAXS). For this purpose, two home-made X-ray scattering cameras were used. The first one is a Bonse-Hart setup specially designed to perform high resolution (ultra-SAXS) and very low angle measurements (Lambard et al., 1992). The second apparatus is a pinhole camera having very high sensitivity for weak scattering systems such as diluted diatom suspensions (Zemb et al., 2003). The measurements were performed in aqueous solution for viable cells and in the air for frustules. The X-ray scattering comes from the scattering length density contrast between two phases. In the case of viable cells in solution, the contrast is taken between the silica skeleton and the organic material layer (which is close to water in term of scattering length density). For dry frustules, the contrast is taken between the silica skeleton and air. Therefore, SAXS cannot resolve the 3-D organic structures on the diatom surface but can be useful for characterizing the specific pores distribution of both dry frustules and viable cultures. The accuracy of pore volume determination is 10%. For the surface determined by the Porod plateau (Spalla, 2003), it can be estimated as 30%.

For diatom frustules in the air, in agreement with SEM images of marine species, a fine porous structure is observed at around 63 nm corresponding to fine pores ≥60 nm in diameter. The signal at large scattering angle is decaying with the fourth power of the angle, which is characteristics of a smooth interface between two materials (Porod

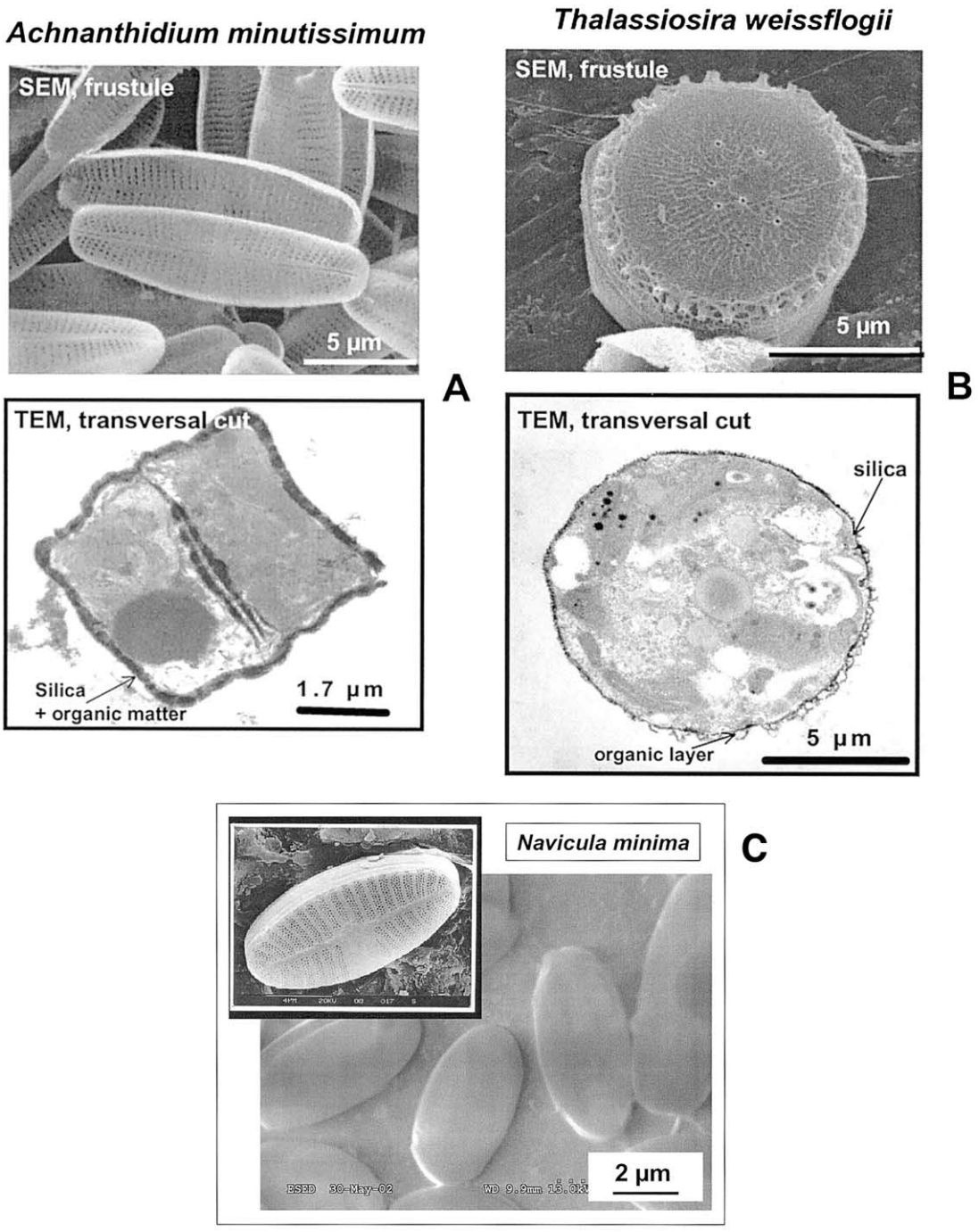

Fig. 1. Representative images of studied diatoms (A) *Achnanthidium minutissimum* (SEM image of frustules and TEM thin section); (B) *Thalassiosira weisflogii* (SEM image of frustules and TEM thin section); (C) Scanning electron micrographs (SEM) of the freshwater periphytic species *Navicula minima*. Upper left: diatom frustule after acid treatment to destroy the organic layer. Main photo: diatoms observed with the variable pressure SEM technique, to preserve the organic layer.

regime, Spalla, 2003). This allows to quantify frustules specific surface areas (in m^2/cell) as listed in Table 1. The total net surface associated with these structures is 44 m^2/g for TW and 67 m^2/g for SC which is about twice lower than those values obtained by BET N_2 measurements. The specific surface area of NMIN and AMIN frustules quantified by SAXS (6 and 13 m^2/g, respectively) are comparable with values of BET N_2 surface measurements (Table 1). The freshwater species AMIN presents a first Porod plateau at 250 nm corresponding to the thickness of the silica shell as also shown by MET images (Fig. 1a). The second Porod plateau at 13 nm corresponds to the surface associated with small size pores on the skeleton visible via SEM. Small size pores ($<$50 nm) have been recently identified in various diatom frustules using small and wide angle X-ray scattering techniques (Vrieling et al., 2000).

Table 2. Experimental conditions of diatom surface titrations in a limited residence time reactor.

Exp. No.	Species	Concentration	Electrolyte	pH range
13	TW	1.1×10^9 cell/L	0.01 M NaCl	3.7–10.0
9, 10	TW	1.1×10^9 cell/L	0.7 M NaCl	3.7–10.6
12	TW	1.1×10^9 cell/L	0.1 M NaCl	3.7–10.4
22	TW	9.3×10^9 cell/L	1 M NaCl	3.0–10.3
25	TW	3.5×10^9 cell/L	0.001 M NaCl	3.0–10.5
26	TW	2.2×10^9 cell/L	1 M NaCl	3.0–10.9
27	TW	2.2×10^9 cell/L	0.001 M NaCl	2.7–10.8
28	TW frustules	2.2×10^9 cell/L	1 M NaCl	1.7–11.4
17	SC	3.2×10^9 cell/L	0.1 M NaCl	3.1–10.3
18	SC	2.7×10^9 cell/L	1 M NaCl	2.8–10.4
19	SC	2.9×10^9 cell/L	0.01 M NaCl	2.6–11.1
11	AMIN	1.7×10^9 cell/L	0.01 M $NaNO_3$	4.0–10.0
M11–14	AMIN	1.0×10^{10} cell/L	0.01 M $NaNO_3$	3.7–10.4
23	AMIN	2.1×10^9 cell/L	0.01 M NaCl	2.8–11.2
30	AMIN	2.1×10^9 cell/L	0.1 M NaCl	3.0–11.0
31	AMIN	8.9×10^9 cell/L	0.1 M NaCl	2.8–11.0
37	AMIN frustules	8.9×10^9 cell/L	0.1 M NaCl	2.6–11.2
20	NMIN	1.55×10^9 cell/L	0.01 M $NaNO_3$	2.3–11.5
21	NMIN	1.48×10^9 cell/L	1 M $NaNO_3$	3.0–10.6

The scattering diagrams for live diatom suspensions and dry frustules are very similar. In accord with results obtained on frustules, the specific surface area of viable cells ranges from 6×10^{-10} m^2/cell for AMIN to 4×10^{-10} m^2/cell for NMIN which is ~10 times lower than corresponding values for marine planktonic species (Table 1). For peryphytic species having low surface area, the accuracy is much lower than for marine ones, in fact, only the bottom value of specific surface area for viable cells can be estimated.

2.2. Surface Titration

Because of the fragility of diatom cell walls and their fast degradation under acid or basic conditions accompanied by release of exudates, conventional batch reactors widely used for the titration of inert mineral oxides or rigid bacterial cell walls are not suitable for diatoms. Preliminary titrations of AMIN, NMIN and TW cells in a batch reactor showed important hysteresis of acid and alkaline titration legs and yield irreproducible results. Besides, the level of dissolved organic carbon (DOC) progressively increases in the course of titration thus making impossible the interpretation of these experiments in terms of net proton adsorption. To overcome these difficulties, a modified limited residence time reactor system (LRT) used for titration of highly reactive solids (Pokrovsky et al., 1999; Pokrovsky and Schott, 2004) was used.

Diatom species were titrated at 25 ± 0.2°C in 0.001 M to 1 mol/L NaCl or $NaNO_3$ solutions and pHs of 3 to 11 (Table 2). Each titration comprised between 20 and 40 data points; altogether, 4, 9, 5 and 2 experiments were performed for SC, TW, AMIN and NMIN species, respectively. The cells were removed from culture media by centrifugation during 10–15 min at 2500 g, rinsed four times with the electrolyte solution and stored during 1 h at 25°C in the dark under N_2 atmosphere and continuous stirring before the titration. For each titration point, a small weighed amount (~5 g) of this homogeneous diatom suspension was transferred to a 8 mL sterile polypropylene vial in which a known amount of titrating solution (standardized NaOH or HCl) was added; pH was recorded once steady state conditions were achieved ($\Delta E/\Delta t \leq 0.5$ and 1 mV/min in the acid and alkaline region, respectively). An aliquot of the solution was filtered for DOC analysis and the remaining part was discarded. This operation was repeated in the whole range of pH chosen. The time of each titrating point acquisition never exceeded 6 min. Optical microscopic inspection of diatoms before and after both the washing and titration runs showed no significant change in the diatoms population. The cells and chloroplasts remained intact and undeformed, and no cell fragments can be detected.

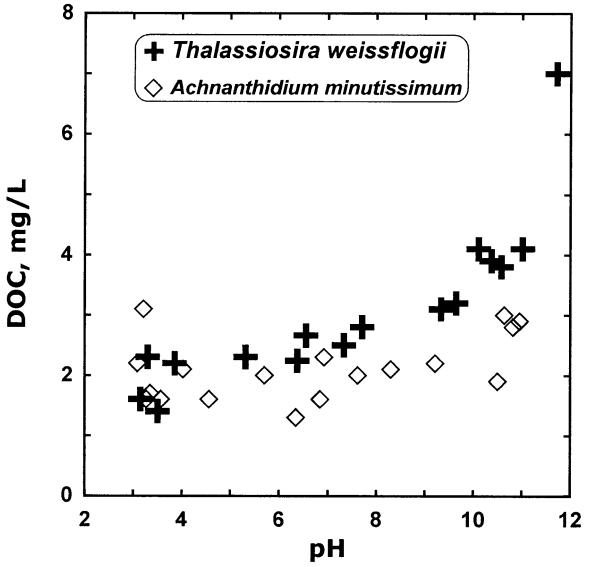

Fig. 2. DOC concentration as a function of pH during diatoms surface titrations. TW = *Thalassiosira weisflogii*; AMIN = *Achnanthidium minutissimum*.

The excess surface proton concentration $[H^+]_S$ at each pH_j titration point (j) was calculated as

$$[H^+]_S = (C_{aj}(\text{suspension}) - C_{aj}(\text{reference})) - (C_{bj}(\text{suspension}) - C_{bj}(\text{reference}) \quad (1)$$

where C_{aj} and C_{bj} correspond to concentrations of base and acid for the jth addition of titrant. For background electrolyte (i.e., $NaNO_3$ or NaCl) C_{aj}(reference) = $[H^+]_j$, free proton concentration in the system, and Eqn. 1 transforms into usual equation used for surface charge calculation from titration data (Cox et al., 1999; Martinez et al., 2002). However, in the case of cell supernatant, C_{aj} (reference) $\geq [H^+]_j$ and $C_{bj} \geq [OH^-]_j$ because of protons and hydroxyls consumption by cell exudates and organic breakdown products in the titrated solution. Therefore, the net surface proton consumption should be corrected for the blank. For this, small volumes of stock suspensions were regularly sampled and centrifuged. The resulting supernatant was titrated under the same conditions as the diatoms suspension and the obtained titration curve was used as a blank allowing the determination of C_{aj} (ref) and C_{bj} (ref) in Eqn. 1. This blank was always subtracted to calculate the net proton adsorption at each pH value. The procedure of surface proton concentration measurements used in this study postulates the "proton condition," i.e., the pH of aqueous suspensions equilibrated with diatom cultures before the titration correspond to zero net proton adsorption or pH_{PZC} (Sposito, 1998).

To assess the degree of cell degradation and the contribution of cell exudates to proton/hydroxyl consumption, the concentration of dissolved organic carbon (DOC) was monitored in the course of titration. Examples of DOC concentration as a function of pH are given in Figure 2. For three diatoms species (AMIN, NMIN and TW), [DOC] remains constant at 2–3 mg/L in the pH range 3–10 thus reflecting a weak degradation of cell walls during titration. *Skeletonema costatum*, in contrast, released an initial amount of DOC ten times higher which further increased during acid titration.

The total amount of protons/hydroxyls consumed during diatoms titration is the sum of H^+/OH^- sunk due to 1) reversible adsorption of H^+/OH^- on the surface layers; 2) irreversible penetration of protons and hydroxyls through the membrane inside the cells; 3) hydrolysis and degradation of the diatom cell wall composites releasing organic compounds in solution, and 4) protonation/deprotonation of initially present dissolved diatom exudates and cell degradation products. If the third and forth processes can be quantified by measuring DOC evolution during titration as well as performing blank supernatant titration, the

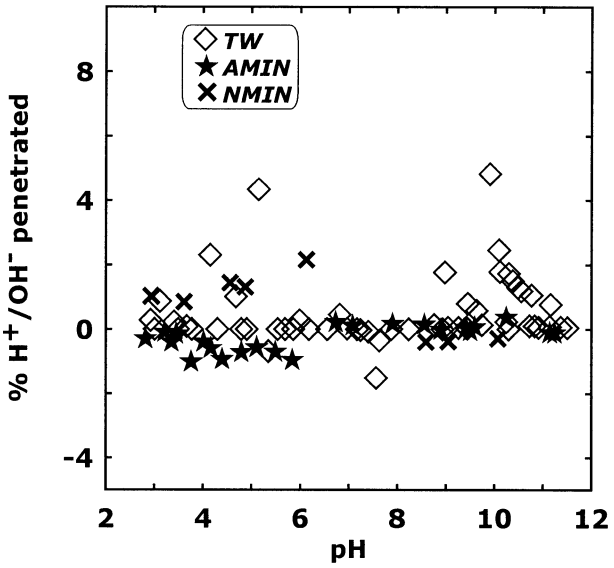

Fig. 3. Proportion of penetrated protons or hydroxyls compared to their total consumption during diatom titrations. TW = *Thalassiosira weisflogii*, AMIN = *Achnanthidium minutissimum*, NMIN = *Navicula minima*.

assessment of H^+ penetration inside the cells required additional experiments. Charge reversibility measurements were performed from stock suspension of each diatom species using the same limited residence time reactor technique, i.e., by adding sequentially, in the 3 to 11 pH range, an equivalent amount of acid or base to each titration vial. The difference between the initial and final pH values taken at ~5 min intervals allowed us to account for the amount of protons incorporated inside the cells according to the equation:

$$[H^+]_{\text{incorporated}} = ([H^+]_{\text{added}} - 10^{-\text{pH(initial)}}/\gamma_{H+}) - ([OH^-]_{\text{added}} - 10^{-\text{pH(final)}}/\gamma_{H+})$$

where [*i*] stands for the concentration of proton or hydroxyl anf γ_H+ is the activity coefficient of aqueous proton. Proportion of incorporated protons or hydroxyls compared to their total consumption during diatom titrations is illustrated in Figure 3. Negligible H^+/OH^- penetration inside the cells (i.e., $\sim 10^{-7}$ M or ≤2%) was observed for AMIN, NMIN and TW. In contrast, *S. costatum* undergoes important penetration of protons and hydroxyls (up to 30–50% of total consumption) which is consistent with its high apparent total charge and elevated DOC concentration measured in the course of titration (not shown).

2.3. Electrophoretic Measurements

Microelectrophoresis is a powerful technique for characterization of the electric double layer (EDL) of microbial cell surfaces (see Richmond and Fisher, 1973) and Van der Wal et al. (1997a) for principles and discussions). In this study, the electrophoretic mobilities of live diatom cells were measured using a microelectrophoremeter ("Zetaphoremeter IV" Z 4000, CAD Instrumentation). Compared to LRT surface titration, the time of contact between aqueous solution and cells in the course of measurements is shorter (up to 1 min) which allows characterization of surface potentials in "extreme" alkaline or acid solutions. The measurements were performed in a quartz channel connecting two Pd electrode chambers. The cells particles were illuminated by a 2 mW He/Ne laser. During the measurements, an electric field of 80 $V \cdot cm^{-1}$ was applied in each direction and the cells movement images were transmitted to a computer via a CCD camera. The electrophoretic mobility of the cells was measured by timed image analysis. Experiments were performed in solutions of ionic strength and pH ranging from 0.001 to 0.1 mol/L (NaCl, HCl) and 1 to 11, respectively. Three replicates were carried out and each of them was performed with a renewed diatoms suspension. The uncertainty attached to electrophoretic mobilities ranged from 5 to 20%, the highest being near the isoelectric point.

2.4. Analytical Methods

Solution pH was measured using a combination glass electrode (Mettler Toledo) calibrated on activity scale with NIST buffers (pH 4.006, 6.865 and 9.18 at 25°C). Precision of pH measurements was ±0.002 U (0.1 mV). Aqueous silica concentration was determined colorimetrically using the molybdate blue method with an uncertainty of 2% and a detection limit of $3 \cdot 10^{-7}$ M. DOC was analyzed using a Carbon Total Analyzer (Shimadzu TOC-5000) with an uncertainty better than 3% and a detection limit of 0.1 ppm.

2.5. X-ray Photoelectron Spectroscopy

X-ray photoelectron spectroscopy is a widespread method for the chemical analyses of solid surfaces. Due to the shallow depth of X-ray beam penetration inside the material (up to 10 nm), this technique allows quantitative elementary analysis of the cell wall layers without interference from the inner compartments of the cell. Nevertheless, XPS has been rarely applied for the analyses of cell surfaces. This may be imputed to difficulties encountered during sample preparation (Marshall et al., 1994); for example, washing of cells in deionized water (MilliQ system) before the analysis may lead to an osmotic shock for marine species (*T. weissflogii* and *S. costatum*). Moreover, due to the high vacuum required for measurements, the sample has to be freeze-dried before analyses which can provoke cell wall breaking during the freezing phase. Note that the pertinence of analyses performed under high vacuum compared to the normal hydrated state of the cell wall can be also questioned. For a review and discussions of validity of XPS measurements for bacterial surfaces, see the works of Dufrène et al. (1997), Rouxhet and Genet (1991) and van der Mei et al. (2000). Note, however, these authors found good agreement between XPS and classical biochemical analyses and good internal reproducibility. In this study, we applied, for the first time, XPS to diatom cell wall characterization. Compared to bacteria, diatoms present a better opportunity of cell walls characterization because, upon liophylization and preparation in vacuum, they are likely to conserve outermost organic layers covering the silica frustule and thus the volume changes accompanying the "collapse" of organic compounds should be minimal. To account for possible cell breakdown during the preparation procedure, we compared the transmission and diffuse reflectance FT-IR spectra of freeze-dried and semidry (almost viable) cells and did not detect any principle differences in band position and intensities.

Each diatom species was rinsed four times in MilliQ water and centrifuged during 20 min at 2500 g; the resulting pellet was frozen and freeze-dried for 24 h. Reference organic compounds (xylose, saccharose, glycine and sorbitol) were subjected to freeze drying together with diatoms samples. Two independent series of measurements were performed for each species. Analyses were conducted on an ESCALAB VG 220i-XL spectrometer. A nonmonochromatic twin Al K_α X-ray radiation ($h\nu = 1486.6$ eV) was used as the excitation source at a power of 200 Watts. Analyzing pass energy of 20 eV with a step size of 0.10 eV was used. The reproducibility of measured atomic ratios for diatom surfaces was better than 10% allowing to quantitatively measure the surface concentrations of carbon, oxygen, nitrogen and silicon.

2.6. FT-IR Spectroscopy

In situ Attenuated Total Reflection (ATR) was employed in this study for diatom surface characterization. Complementary to XPS, this technique allows semiquantitative identification of the chemical nature of organic and inorganic moieties present on the surface of viable cells in aqueous solution (Naumann et al., 1991; Schmitt and Flemming, 1998).

The spectra were recorded on a Bruker IFS88 FTIR spectrometer with a MCT detector by means of an ATR attachment. All the accessories were from Harrick Scientific Co. The spectrometer was purged with CO_2-free dry air (Balston Filter) in a chamber at ~25°C. The spectra were taken at 4 cm^{-1} resolution by coadding up to 200 scans in the 4000–500 cm^{-1} region. The unit of intensity was defined as $-\log(R/R_0)$ where R_0 and R are the reflectivities of the system without and with the investigated medium, respectively. The spectra of cell

Table 3. Penetration depth of evanescent wave in water (μm) for two types of reflection elements at reflection angle of 45°. Optical constants of water in the infrared are from Downing and Williams (1975).

Wave number (cm^{-1})	n H_2O	Ge	ZnSe
2920	1.415	0.223	0.579
1700	1.242	0.368	0.807
1000	1.214	0.623	1.338

supernatant in the background electrolyte ($NaNO_3$) or MQ water were always substracted. ATR spectra were recorded using ZnSe and Ge reflection elements at an incidence angle of 45°C on the diatom suspension. The use of two different detectors allowed us to account for the change of identity and relative proportion of organic groups depending on depth of beam penetration in the cell surface in suspensions: 0.6 to 1.3 μm and 0.2 to 0.6 μm for the ZnSe and Ge reflection elements, respectively (Table 3). An approximation of the refraction index of the organic layers between 1.3 and 1.5 yields the overall uncertainties on our estimation of depth penetration at ~30%. Spectra were recorded for concentrated diatom suspension (~50–100 g humid/L) at pH around 7. The spectra of the different generations of diatom species prepared in the same solution conditions showed very good reproducibility of surface composition.

3. RESULTS

3.1. Spectroscopic Observations

3.1.1. ATR

Infrared spectra allowed us to detect the following organic groups: carboxyl (3400, 1740 and 1400 cm^{-1}), aliphatic (1455, 2850, 2930 and 2960 cm^{-1}), protein (1640, 1540 cm^{-1}), hydroxyl (3400 and 1540 cm^{-1} with interference of water at these particular wavelengths), silica (1250–1100 cm^{-1}, in particular 1072 cm^{-1}) and polysaccharide (1086 cm^{-1}) (Table 4).

ATR spectra brought together in Figures 4, 5, and 6 exhibit the most important differences for absorbance bands at ~1072 cm^{-1} assigned to the stretching vibration of the Si-O-Si group of diatom frustules. For *Skeletonema costatum*, a very low intensity of this band was observed even when using the ZnSe reflection element that has a penetration depth of 1.3 μm. This indicates that SC has a very thick outermost organic layer which precludes interaction of the evanescence wave with the silica skeleton. In contrast, the outermost organic layer of AMIN and NMIN is very thin and the reflected radiation interacts very strongly with the silica skeleton even when using the germanium reflection element (Fig. 4). For *Tallassiosira weisflogii*, the outermost organic layer has an intermediate thickness which results in the most significant differences in the intensities of the absorbance bands recorded with germanium and ZnSe reflection elements (spectra b in Fig. 4). Taking into account the spectral observations obtained with both reflection elements and the calculated values of penetration depths at different frequencies listed in Table 3, it could be estimated that the thickness of TW organic layer is $\sim 400 \pm 200$ nm which is consistent with TEM observations of this study. The outermost organic layer of *S. costatum* has a thickness $>$ 1500 nm whereas that for AMIN and NMIN is around 150 ± 50 nm. It should be noted that infrared reflection spectra of frustules for all four diatom species are very similar and resemble that of amorphous silica (spectra not shown). The relative proportions of silanol moyeties inferred from ATR observations as 1072 cm^{-1} peak height in Figure 4A (i.e., SC $\ll$ TW $\ll$ AMIN $<$ NMIN) are consistent with values of frustule/whole cell ratios (Table 1) measured in this study: 0.24, 0.4, 1 and 4 pmol of Si per cell for SC, TW, AMIN and NMIN, respectively.

Table 4. Results of diatoms analysis by FT-IR. Band attributions were made according to Bellamy (1975) and Colthup et al. (1975).

Functional groups	Band (wavelength, cm^{-1}) at 25°C, ± 5 cm^{-1}	Corresponding structure
Aliphatic	2960	CH_3 asymmetric stretching
	2925	CH_2 asymmetric stretching
	2850	CH_3 symmetric stretching
	1455	C–H bending in CH_2
Proteins	1650	>C=O stretching for primary amids
	1545	N–H bending in amids
Carboxylic acids	~3400	O–H stretching
	1405	C–O stretching in carboxylates
	1735	>C=O stretching of ester or fat acids
Polysaccharides	1086	Ring vibration corresponding to C–O stretching of esters
Hydroxyles	~3400	O–H stretching
	~1540	O–H bending
Silica	Several bands at 1250–1100, 1070, and at 940, 790	Si-O-Si stretching

Important differences in the chemical composition of the surface organic layers have been also observed for the four diatom species. *N. minima* displays a significant amount of carboxyl groups with two characteristic bands at 1742 and 1709 cm^{-1} (Fig. 5, spectrum C). These bands are almost invisible for AMIN (Fig. 5, spectrum D). The band position at 1742 cm^{-1} could suggest the presence of carboxyl groups in form of ester and/or aldehyde (Bellamy, 1975; Colthup et al., 1975). The absorbance bands at ~1640 and 1540 cm^{-1} (Fig. 5) can be assigned to two characteristic vibrations of the amide functional groups known as amide I and amide II bands, respectively (Bellamy, 1975). One can observe differences in these bands intensities, shapes and positions. Changes in band positions suggest different protein and/or amines compositions between diatom species investigated in this study. The amount of proteins is highest in the case of NMIN while it is the same for the three others diatoms. Only in the case of *S. costatum* it is possible to observe characteristic absorbance bands of the organic outermost layer without overlap with the strong absorbance from the silica skeleton (Fig. 6). In this frequency region (900–1700 cm^{-1}), known as the fingerprint of the investigated sample, bands assignments are most difficult. There are three clearly visible absorbance bands at ~1150, 1076 and ~1015 cm^{-1}. These bands could be tentatively assigned to the C-O (the first two bands) and P-O-C molecular groups vibrations. Amine and amide deformation vibrations could be other possible assignments. Detailed spectroscopic chemical characterization of these and other diatom species and their skeletons will be the subject of another report.

3.1.2. XPS

These analyses allow to approximate the concentrations of carbon, oxygen, nitrogen and silicon at the surface of diatoms.

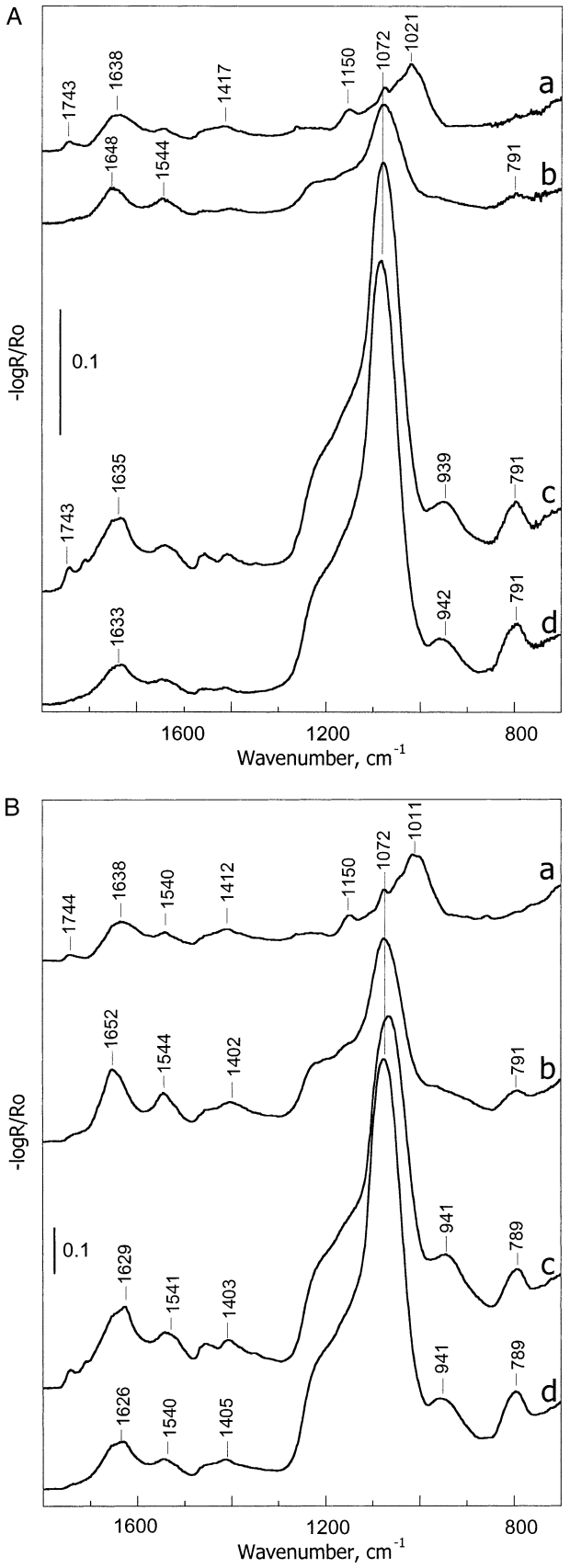

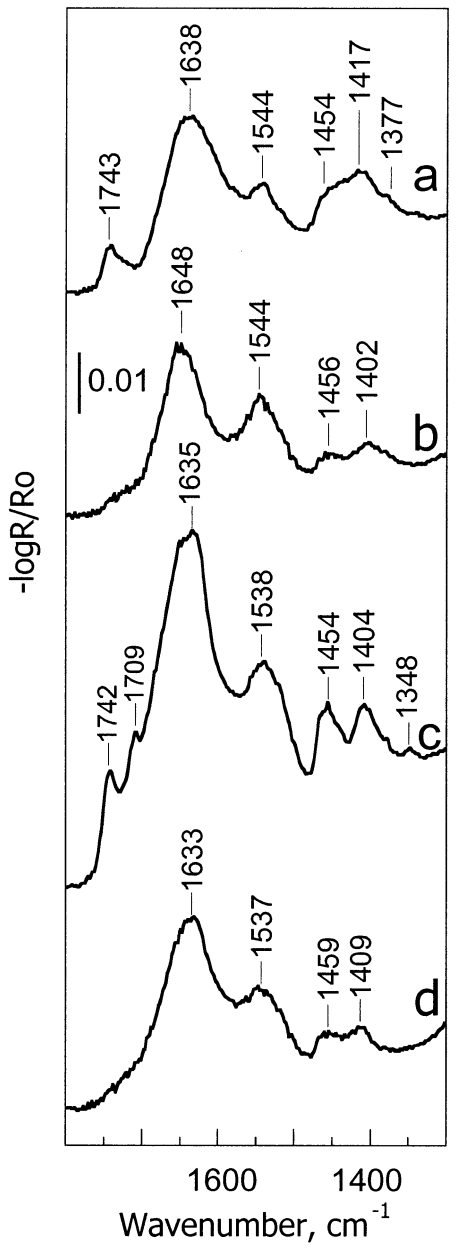

Fig. 5. IR ATR spectra of diatom species recorded with Ge reflection element in the region of carboxyl and amid/amin group vibrations. *a* = *Skeletonema costatum*, b = *Thalassiosira weisflogii*, c = *Navicula minima* and d = *Achnanthidium minutissimum*.

XPS peaks corresponding to P, S and K were occasionally found but they were too weak to allow concentration measurements. The shape of carbon peak was found to be quite similar among different contrasted diatom species (Fig. 7). The surface composition of diatom species as measured by XPS is given in Table 5 which provides the tentative atomic percentage of the

Fig. 4. IR ATR spectra of diatom species recorded with Ge (A) and ZnSe (B) reflection elements. a = *Skeletonema costatum*, b = *Thalassiosira weisflogii*, c = *Navicula minima* and d = *Achnanthidium minutissimum*.

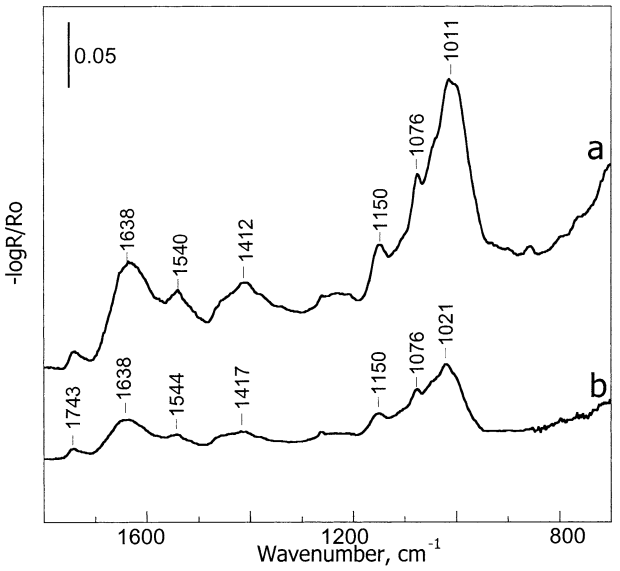

Fig. 6. IR ATR spectra of Skeletonema costatum recorded with ZnSe (a) and Ge (b) reflection elements.

four major elements. The principal constituents of the diatom cell walls are peptidoglycan, polysaccharides, (lipo)polysaccharides, lipids and proteins (Hecky et al., 1973). The surface composition of diatom cell walls can therefore be modeled in terms of three classes of basic constituents: proteins, polysaccharides and hydrocarbon-like compounds. Cell wall molecular composition was computed from elemental concentration ratios using the method developed for bacteria surfaces by Dufrène and Rouxhet (1996) and Dufrène et al. (1997):

$$(N/C)_{observed} = 0.279\ (C_{PE}/C)$$

$$(O/C)_{observed} = 0.325\ (C_{PE}/C) + 0.833\ (C_{PS}/C)$$

$$(C/C)_{observed} = (C_{PE}/C) + (C_{PS}/C) + (C_{HC}/C) = 1$$

where N/C and O/C are nitrogen and oxygen to carbon atomic ratios, and PS, PE and HC stand for polysaccharides, peptides

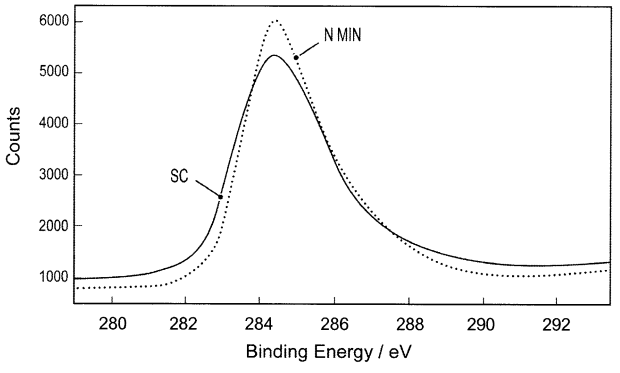

Fig. 7. XPS spectra of carbon for the two most contrasted species. The shape of carbon peak is quite similar for NMIN and SC and very different from the phospholipids of bacterial cell envelopes (Rouxhet and Genet, 1991; Rouxhet et al., 1994; Dufrène et al., 1997) due to the presence of phospholipids in these latter.

Table 5. Atomic percentage of elements in diatoms cell walls as measured by XPS.

Species	C	O	N	Si
SC	72.2	22.3	1.85	2.8
TW	65.7	24.9	5.6	2.4
NMIN	63.3	24.5	4.1	7.6
AMIN	62.15	26.8	2.35	8.15

and hydrocarbon-like compounds, respectively. The resolution of XPS analyses allows quantification of the proportion of these organic molecules for each diatom species (Fig. 8). The validity of this approach was checked by analyzing several reference organic compounds (glycine $C_2H_5NO_2$, aspartic acid $C_4H_7NO_4$, sorbitol $C_6H_{14}O_6$ and xylose $C_5H_{10}O_5$). The difference between measured and calculated concentrations of organic molecules for these compounds never exceeds ±10%. Another method for approximating cell walls chemical composition is the deconvolution of the XPS carbon peak into the contributions corresponding to the three different environments met by carbon: C-(O,N) at 286.3 eV for alcohol, ether, amine and amide; C=O at 287.8 eV for acetal, amide, carboxylate and carbonyl; and C-(C,H) at 284.8 eV for hydrocarbon-like compounds which is used as a reference to calculate the binding energy of all other peaks (Rouxhet et al., 1994; Dengis et al., 1995). For all four species studied, a good agreement within 15% was obtained between the percentage of proteins, amide and aliphatic groups derived from the two above methods.

3.2. Electrokinetic Measurements

The values of diatom electrophoretic mobilities (EM) determined by microelectrophoresis are listed in Appendix A1 and illustrated by Figure 9. All species exhibit negative mobilities at pH $>$ 2 as it is the case for most bacteria and organic

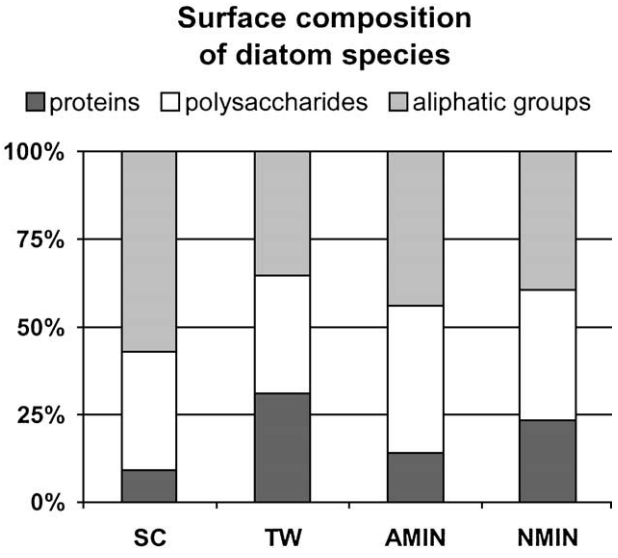

Fig. 8. Surface composition of diatom species expressed in terms of the three major organic compounds measured by XPS.

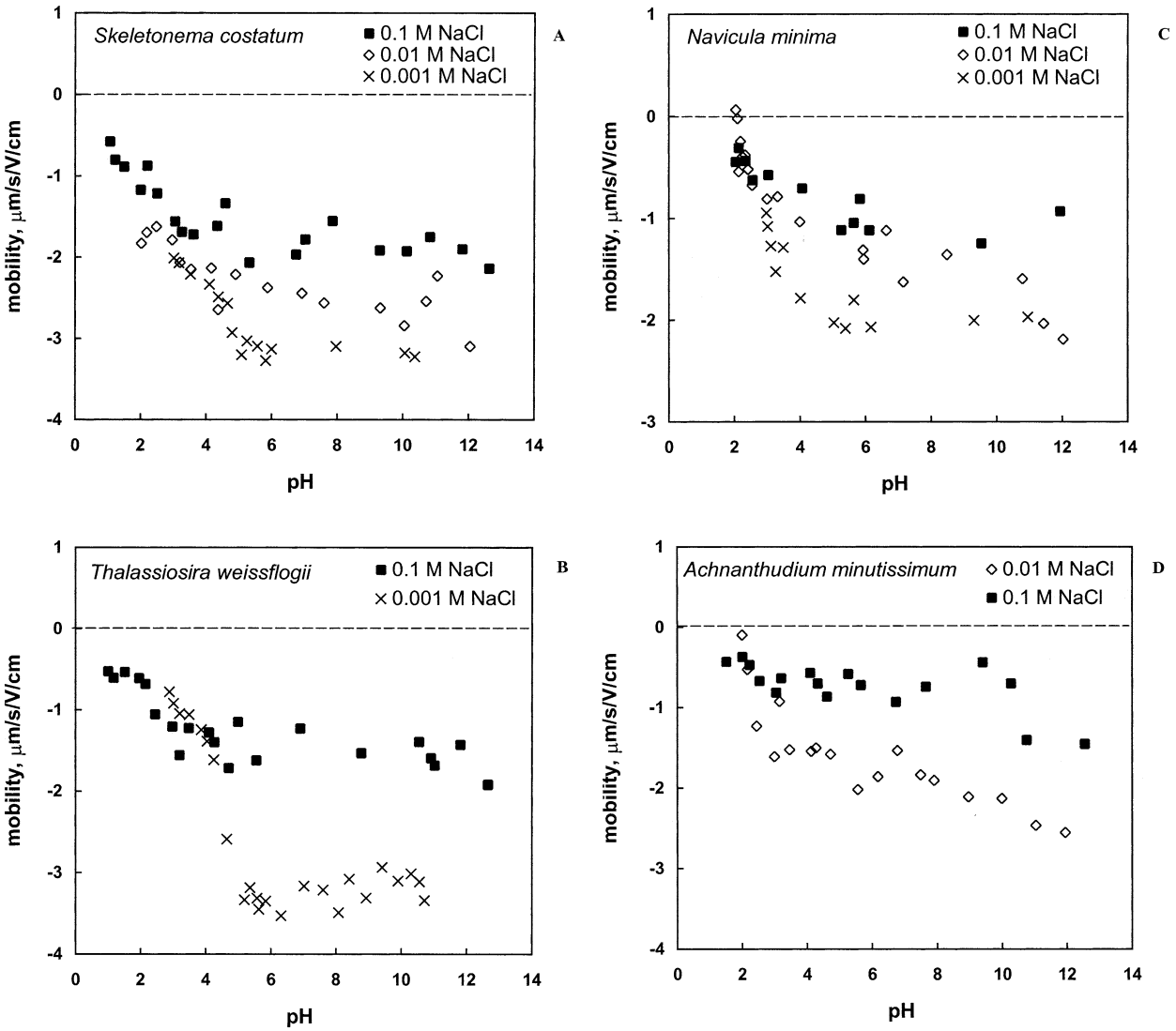

Fig. 9. Electrophoretic mobilities of diatom species. (A) *Skeletonema costatum*; (B) *Thalassiosira weisflogii*, (C) *Navicula minima*, and (D) *Achnanthidium minutissimum*.

surfaces (Richmond and Fisher, 1973; Hayashi et al., 2001). Freshwater diatoms (AMIN and NMIN) exhibit lower EM values compared to the marine species. All four species exhibit similar pH of isoelectric point (pH_{IEP} = 1–2) and EM dependence on pH and ionic strength. EM and ζ-potential of NMIN, TW and SC decrease with pH at pH $<$ 5 and stay constant at 5 $\leq$ pH $\leq$ 11. For AMIN in 0.01 mol/L NaCl, continuous decreases of EM as a function of pH is observed (Fig. 9D). This behavior of diatoms is similar to that of bacteria (Van der Wal et al., 1997a; Hayashi et al., 2001; Shashikala and Raichur, 2002) indicating the presence on the outermost layer of organic groups, such as carboxyls, bearing negative charges. The pH dependences of electrophoretic mobilities for *N. minima* whole cells and their frustules are different: whereas the frustule mobilities decrease semilinearly with pH as it is expected for SiO_2 (Kosmulski et al., 2002), the whole cells mobilities exhibit only a weak dependence on pH at 4 $<$ pH $<$ 9 (Fig. 10).

3.3. Surface Titration

Results of all diatoms titration experiments are listed in Appendix A2. Examples of diatom titrations at different ionic strengths and cell concentrations are presented in Figures 11 and 12. Freshwater diatoms exhibit similar shape of titration curves and close values of their pH_{PZC} (6.4 $\pm$ 0.1 for AMIN vs. 6.3 $\pm$ 0.15 for NMIN). In contrast, the pH dependence of $[H^+]_S$, surface proton concentration, is very different for TW and SC and their pH_{PZC} are equal to 8.2 $\pm$ 0.1 and 9.3 $\pm$ 0.1, respectively. In alkaline solutions, the effect of ionic strength is the most pronounced for NMIN (Fig. 11C). This observation is consistent with a much higher concentration of silanol surface groups for freshwater species compared to marine diatoms and the strong dependence of surface silanol deprotonation on ionic strength (Sverjensky and Sahai, 1996). High uncertainty, up to 30%, can be attributed to $[H^+]_S$ at pH $<$ 3 and pH $>$ 10.5. This is due to the competition between protonation/deprotonation of

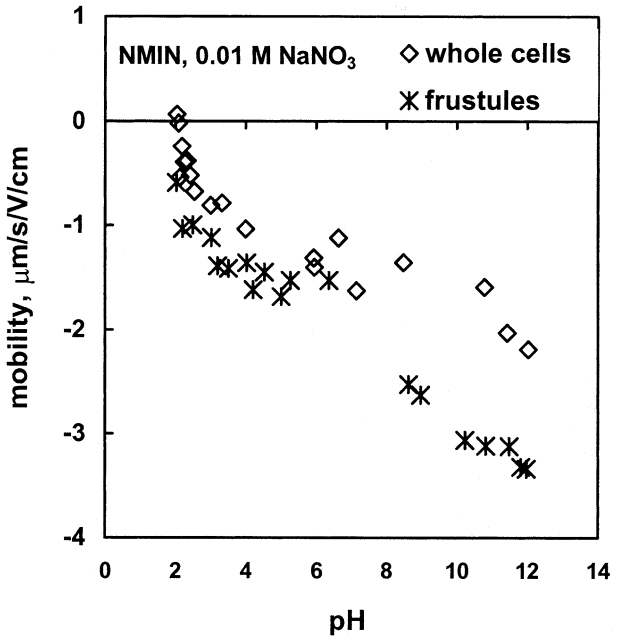

Fig. 10. Comparison between the electrophoretic mobilities of the whole cells *Navicula minima* and their frustules.

dissolved organic ligands (diatom exudates and degradation products of the cell walls) and acid/base reactions on surface groups. The proton consumption associated with frustules, close to zero at pH < 9, is much lower than that of the whole cells. This is illustrated in Figure 12 that presents the pH-dependence of $[H^+]_S$ for the whole TW and AMIN cells and that for the same concentration (i.e., 2.2×10^9 and 8.9×10^9 cell/L, respectively) of their frustules.

3.4. Surface Proton Adsorption Modeling

It follows from our spectroscopic results that carboxyl, amine and silanol moyeties are the three major proton-active surface sites. As a result, the following reactions have been postulated to control the charge at diatoms/aqueous solution interface:

1) protonation of carboxyl groups

$$>COO^- + H^+(aq) = >COOH^\circ \quad pK_{a1} \sim -4\text{–}5 \qquad (1)$$

2) protonation of silanol groups

$$>SiO^- + H^+(aq) = >SiOH^\circ \quad pK_{a2} \sim -7\text{–}8 \qquad (2)$$

3) protonation of amine groups

$$>NH_2^\circ + H^+(aq) = >NH_3^+ \quad pK_{a3} \sim 9.5\text{–}11 \qquad (3)$$

To provide a first-pass description of diatom surface proton adsorption, we have fitted our data using the surface stoichiometries of the active groups derived from XPS measurements. In agreement with previous studies on bacteria and algae, the pK_a of intrinsic surface stability constants for reactions 1–3 were initially fixed as 4.5, 7.5 and 10, respectively. This choice relies on the well-known analogy between surface and solution complexation reactions (Schindler and Stumm, 1987). After this preliminary modeling, either surface stability constants or site densities were allowed to vary by not more than 0.5 log units and 30%, respectively, from initial values to provide a best fit of the experimental dependence of $[H^+]_S$ on pH. When small variations of surface stability constants were not sufficient to provide acceptable fit, they were allowed to vary up to 1 logarithm unit.

Results of surface proton adsorption modeling using FITEQL 3.2 (Herbelin and Westall, 1996) are presented as solid lines in Figures 11 and 12 whereas SCM parameters for the four diatom species are listed in Table 6. Because of high dispersion of experimental titration data points obtained in LRT reactor, the goodness of fit (overall variance V(Y)) remained very low, around 100. For the same reason, the fit with open site concentrations and pK values was not possible. In contrast, the V(Y) parameter for fitting diatoms titrations performed in batch reactors does not exceed 4, however, the interpretation of batch surface titration data for diatoms is not straightforward due to important artifacts affecting proton consumption and titration legs hysteresis (see section 2.2). Therefore, only LRT titration data were used for the fitting procedure. We found that, for AMIN, NMIN and TW, a 3-sites model was a good fit to the data and the addition of new sites (i.e., phosphate or hydroxyl) did not improve the goodness of fit. Two-sites or one-site models could not provide the convergence of fit. For SC, including the silanol groups in surface titration modeling did not allow any better description of data, i.e., two- and three-sites models provided equally good fit.

It can be seen in Figures 11 and 12 that there is a good adherence to experimental data of predicted $[H^+]_S$ as a function of pH. The surface complexation model generated in this study assumes a constant capacitance of the electric double layer, similar to that developed for bacterial surfaces (Fein et al., 1997; Daughney and Fein, 1998; Daughney et al., 1998). In this model, the surface potential is independent of ionic strength; as a result, charge modeling requires a different set of surface protonation constants for each ionic strength investigated. We did not observe a systematic trend in variation of surface groups dissociation reactions constants with ionic strength or this trend is masked by the uncertainties of measurements.

The EDL capacitance value, C, which could not be fitted by FITEQL, was fixed initially for each species and once the other parameters were determined, it was allowed to vary within 30–50% to test the sensitivity of the model to C. The values used for surface proton adsorption modeling are 2500 ± 300, 730 ± 100, 350 ± 50 and 5400 ± 400 F/g_{dry} for AMIN, NMIN, TW and SC, respectively. These values are within the range reported for bacteria (Fein et al., 1997; Daughney and Fein, 1998). Normalization of EDL capacitances to specific surface area of silica skeletons yields values between ~200 (NMIN) and ~500 (SC) F/m^2. Such high capacitances are likely to originate from the multilayer structure of organic constituents of diatom cell walls capable of accommodating high charge densities within relatively short distances. In this regard, C values for porous multilayer diatoms cell walls can be considered as purely adjustable parameters without rigorous physical meaning (i.e., Lützenkirchen, 1999).

The relative proportion of functional groups is nearly the same for the two freshwater species but significantly different for TW and SC. The cell number–normalized ratios of the

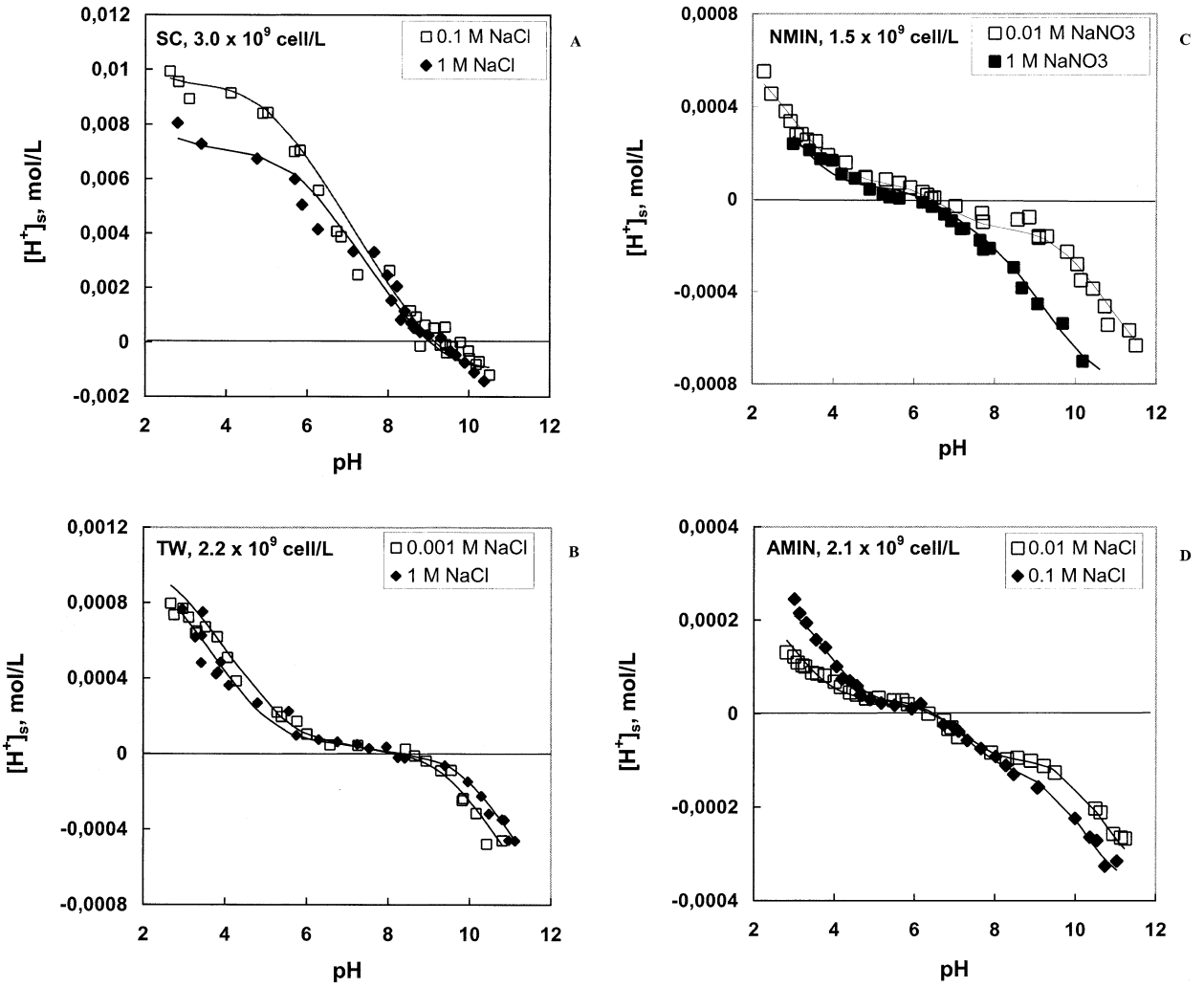

Fig. 11. The excess surface protons concentration of diatom species (mol/L) as a function of pH for *Skeletonema costatum* (A), *Thalassiosira weisflogii* (B), *Navicula minima* (C), and *Achnanthidium minutissimum* (D). The symbols represent results of our experimental titrations, but the curves were generated from the surface complexation model (SCM) proposed in this study using values of sites densities and thermodynamic parameters listed in Table 6.

three major surface sites {>COOH}: {>NH_3}: {>SiOH} are 1:1:0.1, 1:10:0, 1:1:0.4 and 1:1:0.3 for TW, SC, AMIN and NMIN, respectively. The total amount of proton/hydroxyl active surface sites ranges from 1 to 9 mmol/g dry weight for NMIN and SC species, respectively. Note that modeling of AMIN titration at biomass concentration of 8.5 and 35 g/L and fixed ionic strength (Figs. 11D and 12B, respectively), can be performed with the same cell weight-normalized concentration of surface functional groups and almost identical set of surface stability constants.

4. DISCUSSION

The combination of the various spectroscopic and macroscopic techniques employed in the present study provides important insights on the three dimensional structure and chemistry of diatom cell walls. However, because different techniques probe different depth in different ways, their comparison cannot be straightforward and only qualitative correlations between results of different methods are possible.

4.1. Surface Spectroscopy

This study presents the first attempt to use FT-IR and XPS techniques for characterizing diatom surface chemistry. In accord with the scarce data available for algal surfaces (Keifer et al., 1997), algal-dominated biofilms and bacteria (Naumann et al., 1991; Schmitt and Flemming, 1998), carboxylic, aliphatic and amino moyeties are the main reactive surface organic groups identified in this study by the ATR technique. Investigated diatoms do not exhibit any XPS-measurable amount of phosphorus on their surfaces as they contain very low amount of phospholipids on their cell walls compared to amino acids and polysaccharids. This is also confirmed by the shape of the

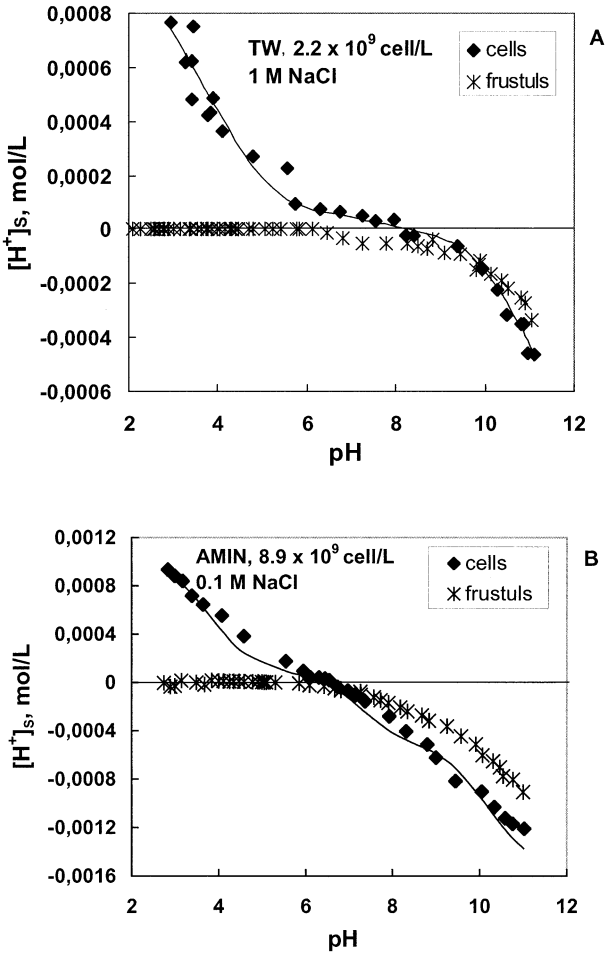

Fig. 12. Quantitative comparison of excess surface proton concentration associated with whole cells and their frustules for equal concentration of cells for TW, I = 1 mol/L NaCl (A) and AMIN, I = 0.1 mol/L NaCl (B). The curves represent the SCM fit to the experimental data.

carbon XPS peak of diatoms (Fig. 7) that is quite similar for the four investigated species but is different from that of bacteria (Rouxhet and Genet, 1991; Rouxhet et al., 1994; Dufrène et al., 1997) whose cell wall comprises a significant amount of phospholipids.

The Si/C ratios measured by XPS (Table 5) and the relative intensity of Si-O-Si bands estimated from the ATR spectra of studied diatoms (Figs. 4 and 5) are in good agreement with frustule/whole cells mass ratios measured in the present work (Table 1) and reported in literature (Conley et al., 1989). In particular, cell walls of planktonic diatoms contain ~5 times less silica than those of periphytic species. A quantitative comparison between surface groups concentration determined by spectroscopic techniques and modeling of surface charge data can be assessed in Figure 13 where the percentage of >SiOH, >COOH and $>NH_2$ groups obtained from SCM is correlated with the percentage of Si and proteins in diatoms cell walls determined by XPS. A positive correlation is observed suggesting the consistency between different methods of surface characterization.

Table 6. Surface speciation model of four diatom-water interfaces.[a]

Species	>COOH sites conc. (10^{13} mol/cell)	$>NH_3$ sites conc. (10^{13}mol/cell)	>SiOH sites conc. (10^{13} mol/cell)	Total sites (mmol/cell)	Total sites (mmol/g dry cell)	Total sites (mmol/m^2 frustules)	EDL capacitance (μF/cell)	>COOH pK_{a1}			>NH_3 pK_{a3}			>SiOH pK_{a2}		
								1 M	0.1 M	0.01 M	0.001 M	1 M	0.1 M	0.01 M	0.001 M	1 M	0.1 M	0.01 M	0.001 M
TW	4.26 ± 0.08	4.55 ± 0.05	0.48 ± 0.25	9.3×10^{-10}	0.66	0.346	0.49 ± 0.07	−4.9 ± 0.4	−4.2 ± 0.1	−5 ± 0.1	−4.9 ± 0.1	10.15 ± 0.35	9.7 ± 0.1	9.8 ± 0.1	10.1	−7.35 ± 0.15	−7 ± 0.1	−7.5 ± 0.1	−7.5 ± 0.1
SC	2.7 ± 1.4	32 ± 3	0	3.5×10^{-9}	9.5	0.94	2.0 ± 0.35	−4.7 ± 0.1	−4.7 ± 0.1	−4.7 ± 0.1	ND	8.2 ± 0.1	8.2 ± 0.1	8.0 ± 0.1	ND	ND	ND	ND	ND
AMIN	0.96 ± 0.13	1.04 ± 0.15	0.38 ± 0.31	2.4×10^{-10}	1.14	0.187	0.52 ± 0.075	ND	−4 ± 0.1	−3.5 ± 0.3	ND	ND	9.8 ± 0.1	10.5 ± 0.3	ND	ND	−7.2 ± 0.1	−6.8 ± −0.2	ND
NMIN	3.9 ± 0.2	4.3 ± 0.1	1.3 ± 0.3	9.5×10^{-10}	0.95	0.28	0.73 ± 0.1	−3.2 ± 0.1	ND	−3.5 ± 0.1	ND	8.5 ± 0.1	ND	10.1 ± 0.1	ND	−6.5 ± 0.1	ND	−7.0 ± 0.1	ND

[a] ND = not determined.

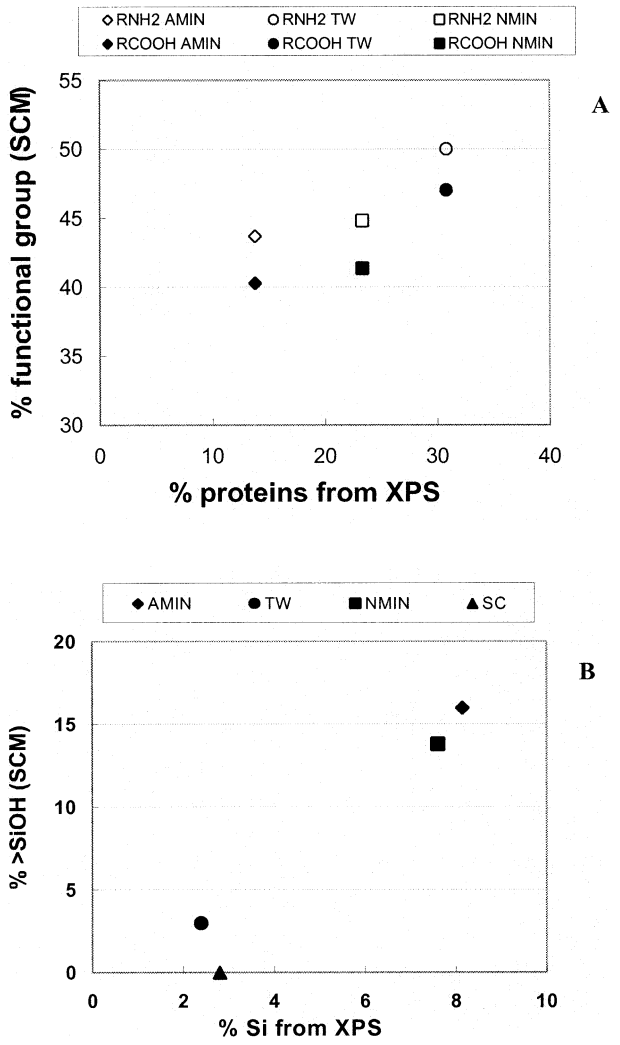

Fig. 13. Comparison between surface groups concentration determined by XPS and obtained from surface titrations modeling. (A) Correlation between protein content in the cell walls measured by XPS and percentage of proteins functional groups obtained from SCM; (B) Correlation between atomic percentage of Si measured by XPS and relative proportion of >SiOH° groups deduced from SCM.

4.2. Surface Complexation Model

Diatom surface proton adsorption dependence on pH and weight-normalized surface site densities determined in the present study are similar to those previously reported for marine diatom species (Gonzalez Davila et al., 1995, 2000), spores of marine bacteria (He and Tebo, 1998), freshwater algae (Xue et al., 1988; Keifer et al., 1997), and whole bacteria and their cell walls (Plette et al., 1995; Martinez et al., 2002; Phoenix et al., 2002). Note, however, the important shift between the pH of isoelectric point (pH_{IEP}) measured by electrophoresis and the pH of zero charge point (pH_{PZC}) determined by surface titration (1–2 vs. 6–9). This difference can be understood in view of diatoms cell wall structure proposed by Hecky et al. (1973) based on their chemical analysis. According to this model, the amino groups attached to silica templates are covered by a polysaccharide layer bearing negatively charged carboxylic groups. Reversible protonation/deprotonation of deeper located amine groups is responsible for the high concentration of surface proton excess measured during titration experiments. These groups are situated far from the shear plane and thus cannot contribute to the zeta potential development. The weak proportion of dissociated $>COO^-$ groups on the surface (pK = 4) even at pH 2 is enough to provide a negative zeta potential. The carboxylic groups dominating the outermost surface layer are fully deprotonated at pH > 4–5 thus yielding constant surface potential and pH-independent zeta potential. Note that a two pH units difference between PZC and IEP for bacterium *Rhodococcus erythropolis* has been ascribed to the presence of a thin polysaccharide layer on its surface (Van der Wal et al., 1997a,b). For diatoms, it follows that the thicker the organic layer, the larger the difference between pH_{IEP} and pH_{PZC}. Indeed, this shift is twice lower for AMIN and NMIN compared to marine planctonic species (see sections 2.1.2. and 3.1.1 for cell wall thickness discussion).

In accord with previous data on bacteria (Plette et al., 1995, 1996; Daughney and Fein, 1998), the protonation constant of carboxylic and amine groups determined in this study ranges from 4 to 6 and 8 to 10, respectively. Fitted values for deprotonation constants of freshwater and marine diatom silanol groups (6.5–7.5) are within the range reported for diatom frustules (Dixit and Van Cappellen, 2002), quartz (Duval et al., 2002) and amorphous silica (Sverjensky and Sahai, 1996). Freshwater periphytic diatoms present close values of protonation constants and surface concentrations for the three functional groups (Table 6). The surface stability constant for TW carboxylic groups is lower than that for freshwater species whereas the amino groups protonation constants are quite similar. Silanol groups concentration on TW is ~5 times lower than that on AMIN, in qualitative agreement with XPS and FT-IR results. *S. costatum* presents a quite different surface chemistry. The amino groups protonation constant is significantly lower than that for the peryphytic species whereas $>NH_2$ concentration is much higher. Within the resolution of our surface titrations, the silanol groups concentration on SC is insignificant. Apparently, for SC, a thick layer of proteins/carboxylic acids governs the surface proton adsorption and prevents the silica frustule from contact with the external solution. Unlike for the three other diatom species, proton adsorption on SC is not fully reversible (see section 2.2), as a result, values of site densities and surface stability constants listed in Table 6 for this species should be considered as rough estimates and will not be used for further discussion.

The total concentration of proton- and hydroxyl-active functional groups on AMIN, NMIN and TW surfaces (~1 mmol/g dry weight, Table 6) is comparable with that reported for bacterial cell walls based on numerous surface titrations (0.5–5 mmol/g, Plette et al., 1995; Fein et al., 1997; van der Wal et al., 1997b; Daughney and Fein, 1998; He and Tebo, 1998; Cox et al., 1999; Daughney et al., 2001; Sokolov et al., 2001; Yee and Fein, 2001). Normalization of the total sites density to the B.E.T. surface area of siliceous skeletons yields values between 0.3 and 0.9 mmol/m^2. These numbers are one order of magnitude higher than the maximal surface sites densities for diatom frustules (Dixit and Van Cappellen, 2002) and amorphous silica (Sverjensky and Sahai, 1996). Therefore, the acid-base properties and, possibly, the affinity for metals of diatom cultures are essentially governed by the organic layers covering the silica frustule.

5. CONCLUSIONS

This study reports on a concerted multitechnical approach for characterizing diatoms surface chemistry in aqueous solutions. Following the tracks developed earlier for bacteria, we demonstrate, using a set of conventional macroscopic (surface titration, electrophoresis) and spectroscopic (SEM, TEM, FT-IR and XPS) techniques, that a quantitative thermodynamic approach can be successfully applied to describe chemical equilibria at the diatoms/solution interfaces. This approach allowed us to elucidate important differences in terms of surface charge and surface chemical composition between marine and estuarine planktonic (*T. weisfloggi*, *S. costatum*) and freshwater peryphytic (*A. minutissimum*, *N. minima*) species. In particular, the relative proportion of silica in the cell wall of diatoms is much lower for planktonic than for peryphytic species whereas the polysaccharidic outermost layer is much thicker in marine species. Use of four different species allowed us to correlate the results of spectroscopic (XPS) measurements with surface complexation modeling.

Comparison of pH_{IEP} measured by electrophoresis (≤ 2 and <1 for peryphytic and planktonic species, respectively) and pH_{PZC} obtained by surface titrations (6 and 8 for peryphytic and planktonic species, respectively) suggests that different parts of surface layers participate in surface charge and ζ-potential developments. Such a multilayer organization of the surface structure is also confirmed by surface sites densities measured for diatoms in this study that exceed by more than one order of magnitude the number of sites available on the surface of silica frustules. This suggests the preeminent role of the organic coating in determining the amphoteric properties and the affinity to metals of diatom cell walls.

In natural settings, bacteria degrade the organic membrane of diatoms after their death thus progressively exposing the underlying silica frustules to the aquatic environment. This is accompanied by a dramatic shift in metal binding properties and surface reactivity. For example, up to 90% of totally trapped metals, located in the proton-binding sites of organic coatings (Pokrovsky et al., 2002) are likely to be released in the environment during diagenesis of diatom cells. Moreover, the surface properties of diatom shells (i.e., adsorption of pollutants and dissolution kinetics) are strongly affected by their high surface area and nanoscale porosity. These parameters are likely to considerably evolve in the course of the diagenetic transformations of freshly formed shells into compact diatomite. It is expected that the results of the present study can allow to establish the thermodynamic and structural bases for understanding the molecular mechanisms of metal and toxicant interactions with diatom surfaces and their frustules.

Acknowledgments—We are grateful to J. Fein, H.L. Dong and two anonymous reviewers whose insight and thorough reviews greatly improve the manuscript. This work was supported by the French National Program for Basic Research ACI "Eau et Environnement." We thank B. Etcheverria for invaluble help during diatoms culture process. J.-C. Harrichoury and A. Castillo are thanked for careful technical assistance and BET specific surface area measurements.

Associate editor: J. B. Fein

REFERENCES

Ahner B. A., Morel F. M. M., and Moffett J. W. (1997) Trace metal control of phytochelatin production in coastal waters. *Limnol. Oceanogr.* **42,** 601–608.

Anderson M. A., Morel F. M. M., and Guillard R. R. L. (1978) Growth limitation of a coastal diatom by low zinc ion activity. *Nature* **276,** 70–71.

Bayer M. E. and Sloyer J. L. (1990) The electrophoretic mobility of Gram-negative and Gram-positive bacteria: An electrokinetic analysis. *J. Gen. Microbiol.* **136,** 867–874.

Bellamy L. J. (1975) The Infrared Spectra of Complex Molecules. Chapman and Hall.

Beveridge T. J. (1988) The bacterial surface: General consideration towards design and function. *Can. J. Microbiol.* **34,** 363–372.

Beveridge T. J., Schulze-Lam S. and Thompson J. B. (1995) Detection of anionic sites on bacterial walls, their ability to bind toxic heavy metals and form sedimentale flocs and their contribution to mineralization in natural freshwater environments. In *Metal Speciation and Contamination of Soil* (eds. H. E. Allen, C. P. Huang, G. W. Bailey and A. R. Bowers), pp. 183–205. Lewis.

Beveridge T. J., Hughes M. N., Lee H., Leung K. T., Poole R. K., Savvaidis I., Silver S., and Trevors J. T. (1997) Metal-microbe interactions: Contemporary approaches. *Adv. Microbiol. Physiol.* **38,** 177–243.

Boonaert C. J. P. and Rouxhet P. G. (2000) Surface of lactic acid bacteria: Relationships between chemical composition and physicochemical properties. *Appl. Environ. Microbiol.* **66,** 2548–2554.

Brand L. E., Sunda W. G., and Guillard R. R. L. (1986) Reduction of marine phytoplankton reproduction rates by copper and cadmium. *J. Exp. Mar. Biol. Ecol.* **96,** 225–250.

Busscher H. J., Bellon-Fontaine M.-N., Mozes van der Mei H. C., et al.. (1990) An interlaboratory comparison of physico-chemical methods for studying the surface properties of microorganisms—Application to *Streptococcus thermophilus* and *Leuconostos mesenteroides*. *J. Microbiol. Methods* **12,** 101–115.

Colthup N. B., Daly L. H., and Wiberley S. E. (1975) Introduction to Infrared and Raman Spectroscopy. Academic Press.

Conley D. J., Kilham S. S., and Theriot E. (1989) Differences in silica content between marine and freshwater diatoms. *Limnol. Oceanogr.* **34,** 205–213.

Cox J. S., Smith S., Warren L. A., and Ferris F. G. (1999) Characterizing heterogeneous bacterial surface functional groups using discrete affinity spectra for proton binding. *Environ. Sci. Technol.* **33,** 4514–4521.

Crist R. H., Oberholser K., Shank N., and Nguyen M. (1981) Nature of bonding between metallic ions and algal cell walls. *Environ. Sci. Technol.* **15,** 1212–1217.

Crist R. H., Oberholser K., Schwartz D., Marzoff J., Ryder D., and Crist D. R. (1988) Interactions of metals and protons with algae. *Environ. Sci. Technol.* **22,** 750–766.

Crist R. H., Martin J. R., Guptill P. W., Eslinger J. M., and Crist D. R. (1990) Interaction of metals and protons with algae. 2. Ion exchange in adsorption and metal displacement by protons. *Environ. Sci. Technol.* **24,** 337–342.

Crist R. H., Oberholser K., McGarrity J., Crist D. R., Johnson J. K., and Brittsan J. M. (1992) Interaction of metals and protons with algae. 3. Marine algae, with emphasis on lead and aluminium. *Environ. Sci. Technol.* **26,** 496–502.

Csogor Z., Melgar D., Schmidt K., and Posten C. (1999) Production and particle characterization of the frustules of *Cyclotella cryptica* in comparison with siliceous earth. *J. Biotechnol.* **70,** 71–75.

Daughney C. J. and Fein J. B. (1998) The effect of ionic strength on the adsorption of H^+, Cd^{2+}, Pb^{2+}, and Cu^{2+} by *Bacillus subtillis* and *Bacilluus licheniformis*: A surface complexation model. *J. Coll. Interface Sci.* **198,** 53–77.

Daughney C. J., Fein J. B., and Yee N. (1998) A comparison of the thermodynamics of metal adsorption onto two common bacteria. *Chem. Geol.* **144,** 161–176.

Daughney C. J., Fowle D. A., and Fortin D. E. (2001) The effect of growth phase on proton and metal adsorption by *Bacillus subtilis*. *Geochim. Cosmochim. Acta* **65,** 1025–1035.

Dauta A. (1982) Conditions de développement du phytoplancton: Etude comparative du comportement de huit espèces en culture. I. Détermination des paramètres de croissance en fonction de la lumière et de la température. *Ann. Limnol.* **18,** 217–262.

Dengis P. B., Gerin P. A., and Rouxhet P. G. (1995) X-ray photoelectron spectroscopy analysis of biosurfaces: Examination of performances with yeast cells and related model compounds. *Colloids Surf. B Biointerfaces* **4,** 199–211.

Dixit S. and Van Cappellen P. (2002) Surface chemistry and reactivity of biogenic silica. *Geochim. Cosmochim. Acta* **66,** 2559–2568.

Downing H. D. and Williams D. (1975) Optical constants of water in the infrared. *J. Geophys. Res.* **80,** 1656–1661.

Dufrène Y. F. and Rouxhet P. G. (1996) X-ray photoelectron spectroscopy analysis of the surface composition of Azospirillum brasilense in relation to growth conditions. *Colloids Surf. B Biointerfaces* **7,** 271–279.

Dufrène Y., van der Wal A., and Rouxhet P. G. (1997) XPS analysis of isolated walls and whole cells of five Gram-positive strains. *J. Bacteriol.* **179,** 1–6.

Duval Y., Mielczarski J. A., Pokrovsky O. S., Mielczarski E., and Ehrhardt J. J. (2002) Evidence of the existence of three types of species at the quartz-aqueous solution interface at pH 0–10: XPS surface group quantification and surface complexation modeling. *J. Phys. Chem. B* **106,** 2937–2945.

Fein J. B., Daughney C. J., Yee N., and Davis T. A. (1997) A chemical equilibrium model for metal adsorption onto bacterial surfaces. *Geochim. Cosmochim. Acta* **61,** 3319–3328.

Fisher N. S. (1986) On the reactivity of metals for marine phytoplankton. *Linmol. Oceanogr.* **31,** 443–449.

Fisher N. S. and Fabris J. G. (1982) Complexation of Cu, Zn, and Cd by metabolites excreted from marine diatoms. *Mar. Chem.* **11,** 245–255.

Fisher N. S. and Reinfelder J. R. (1995). The trophic transfer of metals in marine systems. In *Metal Speciation and Bioavailability in Aquatic Systems* (eds. A. Tessier and D. R. Turner), pp. 363–406. Wiley.

Gold C., Feurtet-Mazel A., Coste M., and Boudou A. (2002) Field transfer of periphytic diatom communities to assess short-term structural effects of metals (Cd, Zn) in rivers. *Water Res.* **36,** 3654–3664.

Gold C., Feurtet-Mazel A., Coste M., and Boudou A. (2003) Effect of cadmium stress on peryphytic diatom communities in indoor artificial streams. *Freshwater Biol.* **48,** 316–328.

Goncalves M. L. S., Sigg L., Reutlinger M., and Stumm W. (1987) Metal ion binding by biological surfaces: Voltametric assessment in the presence of bacteria. *Sci. Total Environ.* **60,** 105–119.

Goncalves M. L. S. and Lopez da Conceicao A. C. (1989) Metal ion binding of copper(II), zinc(II), and lead(II) by the algae *Selenastrum capricornutum* Printz. *Sci. Total Environ.* **38,** 155–166.

Gonzalez-Davila M. (1995) The role of phytoplankton cell on the control of heavy metal concentrations in seawater. *Mar. Chem.* **48,** 215–236.

Gonzales-Davila M., Santana-Casiano J. M., Perez-Pena J., and Millero F. J. (1995) Binding of Cu(II) to the surface and excudates of the alga *Dunaliela tertiolecta* in seawater. *Environ. Sci. Technol.* **29,** 289–301.

Gonzales-Davila M., Santana-Casiano J. M., and Laglera L. M. (2000) Copper adsorption in diatom cultures. *Mar. Chem.* **70,** 161–170.

Guillard R. R. L. (1975) Culture of phytoplankton for feeding marine invertebrates. In *Culture of Marine Invertebrate Animals* (eds. W. L. Smith and M. H. Chanley), pp. 26–60. Plenum Press.

Hayashi H., Tsuneda S., Hirata A., and Sasaki H. (2001) Soft particle analysis of bacterial cells and its interpretation of cell adhesion behaviors in terms of DLVO theory. *Colloids Surf. B Biointerfaces* **22,** 149–157.

He L. M. and Tebo B. M. (1998) Surface charge properties of and Cu(II) adsorption by spores of the marine *Bacillus* sp. strain SG-1. *Appl. Environ. Microbiol.* **64,** 1123–1129.

Hecky R. E., Mopper K., Kilham P., and Degens E. T. (1973) The amino acid and sugar composition of diatom cell-walls. *Mar. Biol.* **19,** 323–331.

Herbelin A. L. and Westall J. C. (1996) FITEQL version 3.2, a computer program for determination of chemical equilibrium constants from experimental data. Department of Chemistry, Oregon State University, Corvallis.

Kates M. and Volcani B. E. (1968) Studies on the biochemistry and fine structure of silica shell formation in diatoms. *Z. Pflanzenphysiol. Bd.* **60,** 19–29.

Keifer E., Sigg L., and Schosseler P. (1997) Chemical and spectroscopic characterization of algae surfaces. *Environ. Sci. Technol.* **31,** 759–764.

Kijlstra J. and van der Wal A. (1995) Electrokinetic behaviour of bacterial suspensions. *Bioelectrochem. Bioenergetics* **37,** 149–151.

Kosmulski M., Maczka E., Janusz W., and Rosenholm J. B. (2002) Multiintsrumental study of the electrophoretic mobility of quartz. *J. Coll. Interface Sci.* **250,** 99–103.

Kroger N., Bergsdorf Ch., and Sumper M. (1994) A new calcium binding glycoprotein family constitutes a major diatom cell wall component. *EMBO J.* **13,** 4676–4683.

Lambard J., Lesieur P., and Zemb Th. (1992) A triple axis double crystal multiple reflexion camera used for small angle X-ray scattering. *J. Physique I France* **1192,** 1191–1213.

Ledin M. (2000) Accumulation of metals by microorganisms—Processes and importance for soil systems. *Earth-Sci. Rev.* **51,** 1–31.

Lützenkirchen J. (1999) The constant capacitance model and variable ionic strength: An evaluation of possible applications and applicability. *J. Coll. Interface Sci.* **217,** 8–18.

Marshall K. C., Pembrey R., and Schneider R. P. (1994) The relevance of X-ray photoelectron spectroscopy for analysis of microbial cell surfaces: A critical view. *Colloids Surf. B Biointerfaces* **2,** 371–376.

Martinez R. E., Smith D. S., Kulczycki E., and Ferrsi G. F. (2002) Determination of intrinsic bacterial surface acidity constants using a Donnan shell model and a continuous pK_a distribution method. *J. Coll. Interface Sci.* **253,** 130–139.

Morel F. M. M., Hudson R. J. M., and Price N. M. (1991) Limitation of productivity by trace metals in the sea. *Limnol. Oceanogr.* **36,** 1742–1755.

Morel F. M. M., Reinfelder J. R., Roberts S. B., Chamberlan C. P., Lee J. G., and Yee D. (1994) Zinc and carbon colimitation of marine phytoplankton. *Nature* **269,** 740–742.

Naumann D., Helm D., and Labischinski H. (1991) Microbial characterization by FTIR spectroscopy. *Nature* **351,** 81–82.

Phoenix V. R., Martinez R. E., Konhauser K. O., and Ferris F. G. (2002) Characterization and implications of the cell surface reactivity of Calothrix sp. Strain KC97. *Appl. Environ. Microbiol.* **68,** 4827–4834.

Pistocchi R., Mormile A. M., Guerrini F., Isani G., and Boni L. (2000) Increased production of extra- and intracellular metal-ligands in phytoplankton exposed to copper and cadmium. *J. Appl. Phycol.* **12,** 469–477.

Plette A. C. C., van Riemsdijk W. H., Benedetti M. F., and van der Wal A. (1995) pH dependent charging behavior of isolated cell walls of a gram-positive soil bacterium. *J. Coll. Interface Sci.* **173,** 354–363.

Plette A. C. C., Benedetti M. F., and van Riemsdijk W. H. (1996) Competitive binding of protons, calcium, cadmium, and zinc to isolated cell walls of a gram-positive soil bacterium. *Environ. Sci. Technol.* **30,** 1902–1910.

Pokrovsky O. S., Schott J., and Thomas F. (1999) Processes at the magnesium-bearing carbonates/solution interface. I. A surface speciation model of magnesite. *Geochim. Cosmochim. Acta* **63,** 863–880.

Pokrovsky O. S., Gelabert A., Viers J., Schott J., Boudou A., and Feurtet-Mazel A. (2002) Study of diatoms/aqueous solution interface. II. Interaction of trace metals (Zn, Cu, Cd, Pb, Cr, Al) with freshwater and marine diatoms (abstract 15A). *Geochim. Cosmochim. Acta* **66 (***Suppl.***),** A609.

Pokrovsky O. S. and Schott J. (2004) Experimental study of brucite dissolution and precipitation in aqueous solutions: Surface speciation and chemical affinity control. *Geochim. Cosmochim. Acta* **68,** 31–45.

Richmond D. V. and Fisher D. J. (1973) The electrophoretic mobility of micro-organisms. *Adv. Microbiol. Physiol.* **9,** 1–27.

Rouxhet P. G. and Genet M. J. (1991) Chemical composition of the microbial cell surface by X-ray photoelectron spectroscopy. In *Microbial Cell Surface Analysis: Structural and Physicochemical*

Methods (eds. N. Mozes, P. S. Handley, H. J. Busscher and P. G. Rouxhet), pp. 173–220. VCH.

Rouxhet P. G., Mozes N., Dengis P. B., Dufrene Y. F., Gerin P. A., and Genet M. J. (1994) Application of X-ray photoelectron spectroscopy to microorganisms. *Colloids Surf. B Biointerfaces* **2,** 347–369.

Schindler P. W. and Stumm W. (1987) The surface chemistry of oxides, hydroxides and oxide minerals. In *Aquatic Surface Chemistry* (ed. W. Stumm), pp. 337–365. Wiley.

Schmitt J. and Flemming H.-C. (1998) FTIR-spectroscopy in microbial and material analysis. *Int. Biodetiorat. Biodegrad.* **41,** 1–11.

Schmitt D., Muller A., Csogor Z., Frimmel F. H., and Posten C. (2001) The adsorption kinetics of metal ions onto different microalgae and siliceous earth. *Water Res.* **35,** 779–785.

Shashikala A. R. and Raichur A. M. (2002) Role of interfacial phenomena in determining adsorption of *Bacillus polymyxa* onto hematite and quartz. *Collids Surf. B. Biointerfaces* **24,** 11–20.

Sokolov I., Smith D. S., Henderson G. S., Gorby Y. A., and Ferris F. G. (2001) Cell surface electrochemical heterogeneity of the Fe(III)-reducing bacteria *Shewanella putrefaciens*. *Environ. Sci. Technol.* **35,** 341–347.

Spalla O. (2003) General theorems in small-angle scattering. In *Neutons, X-rays and Light* (eds. P. Lindner and Th. Zemb), pp. 49–71, North-Holland Delta Series, Elsevier.

Sposito G. (1998) On points of zero charge. *Environ. Sci. Technol.* **32,** 2815–2819.

Sunda W. G. and Huntsman S. A. (1995) Regulation of copper concentration in the oceanic nuctricline by phytoplankton uptake and regeneration cycles. *Limnol. Oceanogr.* **40,** 135–137.

Sunda W. G. and Huntsman S. A. (1998) Processes regulating cellular metal accumulation and physiological effects: Phytoplankton as model systems. *Sci. Total Environ.* **219,** 165–181.

Sverjensky D. and Sahai N. (1996) Theoretical prediction of single-site surface-protonation equilibrium constants for oxides and silicates in water. *Geochim. Cosmochim. Acta* **60,** 3773–3797.

Swift D. M. and Wheeler A. P. (1992) Evidence of an organic matrix from diatom biosilica. *J. Phycol.* **28,** 202–209.

Ulberg Z. R. and Marochko L. G. (1999) The electrophoretic properties and stability of the cell suspensions. *Colloids Surf. A. Physicochem. Engng Asp.* **159,** 513–518.

van der Mai H. C., de Vries J., and Busscher H. J. (2000) X-ray photoelectron spectroscopy for the study of microbial cell surfaces. *Surface Sci. Rep.* **39,** 1–24.

van der Wal A., Minor M., Norde W., Zehnder A. J. B., and Lyklema J. (1997a) Electrokinetic potential of bacterial cells. *Langmuir* **13,** 165–171.

van der Wal A., Norde W., Zehnder A. J. B., and Lyklema J. (1997b) Determination of the total charge in the cell walls of Gram-positive bacteria. *Colloids Surf. B. Biointerfaces* **9,** 81–100.

Volesky B. and Holan Z. R. (1995) Biosorption of heavy metals. *Biotechnol. Prog.* **11,** 235–250.

Vrieling E. G., Beelen T. P. M., Van Santen R. A., and Gieskes W. W. C. (1999) Diatom silicon biomineralization as an inspirational source of new approaches to silica production. *J. Biotechnol.* **70,** 39–51.

Vrieling E. G., Beelen T. P. M., van Santen R. A., and Gieskes W. W. C. (2000) Nanoscale uniformity of pore architecture in diatomaceous silica: A combined small and wide angle X-ray scattering study. *J. Phycol.* **36,** 146–159.

Xue H.-B., Stumm W., and Sigg L. (1988) The binding of heavy metals to algal surfaces. *Water Res.* **22,** 917–926.

Yee N. and Fein J. (2001) Cd adsorption onto bacterial surfaces: A universal adsorption edge? *Geochim. Cosmochim. Acta* **65,** 2037–2042.

Zemb Th., Taché O., Né F., and Spalla O. (2003) Improving sensitivity of a small angle X-ray scattering camera with pinhole collimation using separated optical elements. *Rev. Sci. Instrum.* **74,** 2456–2462.

Zhou X. and Wangersky P. J. (1989) Production of copper-complexing organic ligands by the marine diatom *Phaeodactylum tricornutim* in a cage culture turbidostat. *Mar. Chem.* **26,** 239–259.

Appendix 1. Summary of electrophoretic measurements performed in NaCl solutions.

I,M	pH	Mobility (μm/S/V/cm)	Diatoms/frustules
0.001 M	3.02	−2.01	SC
0.001 M	3.18	−2.07	SC
0.001 M	3.53	−2.21	SC
0.001 M	4.11	−2.33	SC
0.001 M	4.38	−2.49	SC
0.001 M	4.80	−2.93	SC
0.001 M	5.57	−3.09	SC
0.001 M	5.09	−3.20	SC
0.001 M	4.66	−2.56	SC
0.001 M	5.25	−3.03	SC
0.001 M	5.82	−3.27	SC
0.001 M	6.00	−3.13	SC
0.001 M	10.37	−3.22	SC
0.001 M	10.07	−3.18	SC
0.001 M	7.97	−3.10	SC
0.01 M	2.03	−1.83	SC
0.01 M	2.19	−1.69	SC
0.01 M	2.49	−1.62	SC
0.01 M	2.97	−1.79	SC
0.01 M	3.21	−2.06	SC
0.01 M	3.55	−2.15	SC
0.01 M	4.17	−2.13	SC
0.01 M	4.37	−2.64	SC
0.01 M	4.90	−2.21	SC
0.01 M	5.88	−2.37	SC
0.01 M	12.05	−3.10	SC
0.01 M	10.72	−2.54	SC
0.01 M	7.61	−2.56	SC
0.01 M	6.93	−2.44	SC
0.01 M	11.06	−2.23	SC
0.01 M	10.05	−2.84	SC
0.01 M	9.32	−2.62	SC
0.1 M	1.06	−0.58	SC
0.1 M	1.22	−0.80	SC
0.1 M	1.50	−0.89	SC
0.1 M	2.00	−1.17	SC
0.1 M	2.20	−0.88	SC
0.1 M	2.51	−1.22	SC
0.1 M	3.06	−1.56	SC
0.1 M	3.27	−1.69	SC
0.1 M	3.62	−1.72	SC
0.1 M	4.34	−1.62	SC
0.1 M	4.59	−1.34	SC
0.1 M	5.32	−2.07	SC
0.1 M	7.03	−1.78	SC
0.1 M	12.63	−2.14	SC
0.1 M	11.82	−1.90	SC
0.1 M	10.83	−1.75	SC
0.1 M	10.12	−1.93	SC
0.1 M	7.86	−1.56	SC
0.1 M	6.75	−1.97	SC
0.1 M	9.30	−1.92	SC
0.001 M	2.89	−0.78	TW
0.001 M	3.01	−0.92	TW
0.001 M	3.21	−1.05	TW
0.001 M	3.49	−1.06	TW
0.001 M	3.87	−1.25	TW
0.001 M	4.04	−1.39	TW
0.001 M	4.25	−1.62	TW
0.001 M	4.65	−2.59	TW
0.001 M	5.84	−3.35	TW
0.001 M	5.36	−3.18	TW
0.001 M	5.58	−3.31	TW
0.001 M	5.64	−3.45	TW
0.001 M	5.19	−3.34	TW
0.001 M	7.02	−3.16	TW
0.001 M	6.31	−3.53	TW

Appendix 1. (Continued)

I,M	pH	Mobility (μm/S/V/cm)	Diatoms/frustules
0.001 M	10.71	−3.34	TW
0.001 M	10.56	−3.11	TW
0.001 M	10.30	−3.01	TW
0.001 M	9.42	−2.94	TW
0.001 M	7.61	−3.21	TW
0.001 M	8.93	−3.31	TW
0.001 M	8.41	−3.08	TW
0.001 M	8.08	−3.49	TW
0.001 M	9.91	−3.10	TW
0.1 M	1.00	−0.53	TW
0.1 M	1.17	−0.61	TW
0.1 M	1.52	−0.53	TW
0.1 M	1.95	−0.61	TW
0.1 M	2.15	−0.68	TW
0.1 M	2.45	−1.06	TW
0.1 M	2.98	−1.21	TW
0.1 M	4.26	−1.40	TW
0.1 M	4.99	−1.15	TW
0.1 M	3.20	−1.56	TW
0.1 M	3.49	−1.23	TW
0.1 M	4.10	−1.28	TW
0.1 M	5.55	−1.62	TW
0.1 M	12.65	−1.92	TW
0.1 M	11.81	−1.43	TW
0.1 M	10.91	−1.60	TW
0.1 M	4.71	−1.72	TW
0.1 M	6.90	−1.23	TW
0.1 M	10.54	−1.40	TW
0.1 M	11.02	−1.69	TW
0.1 M	8.78	−1.54	TW
0.001 M	2.98	−0.95	NMIN
0.001 M	3.02	−1.08	NMIN
0.001 M	3.12	−1.27	NMIN
0.001 M	3.27	−1.52	NMIN
0.001 M	3.50	−1.29	NMIN
0.001 M	4.01	−1.78	NMIN
0.001 M	5.40	−2.08	NMIN
0.001 M	5.04	−2.02	NMIN
0.001 M	5.65	−2.08	NMIN
0.001 M	10.95	−1.97	NMIN
0.001 M	9.31	−2.00	NMIN
0.001 M	6.17	−2.07	NMIN
0.01 M	3.32	−0.79	NMIN
0.01 M	4.00	−1.03	NMIN
0.01 M	3.01	−0.81	NMIN
0.01 M	2.55	−0.67	NMIN
0.01 M	2.42	−0.52	NMIN
0.01 M	2.34	−0.38	NMIN
0.01 M	2.25	−0.39	NMIN
0.01 M	2.19	−0.24	NMIN
0.01 M	2.14	−0.54	NMIN
0.01 M	2.10	−0.02	NMIN
0.01 M	2.05	0.07	NMIN
0.01 M	10.79	−1.59	NMIN
0.01 M	8.48	−1.36	NMIN
0.01 M	6.64	−1.12	NMIN
0.01 M	12.03	−2.19	NMIN
0.01 M	11.43	−2.03	NMIN
0.01 M	7.15	−1.62	NMIN
0.01 M	5.94	−1.31	NMIN
0.01 M	5.95	−1.40	NMIN
0.1 M	2.04	−0.46	NMIN
0.1 M	2.14	−0.31	NMIN
0.1 M	2.34	−0.44	NMIN
0.1 M	2.56	−0.62	NMIN
0.1 M	3.04	−0.58	NMIN
0.1 M	4.07	−0.71	NMIN
0.1 M	5.26	−1.11	NMIN

Appendix 1. (Continued)

I,M	pH	Mobility (μm/S/V/cm)	Diatoms/frustules
0.1 M	5.65	−1.05	NMIN
0.1 M	5.83	−0.81	NMIN
0.1 M	11.94	−0.93	NMIN
0.1 M	9.54	−1.25	NMIN
0.1 M	6.12	−1.12	NMIN
0.01 M	2.03	−0.59	frust NMIN
0.01 M	2.21	−1.03	frust NMIN
0.01 M	2.50	−1.00	frust NMIN
0.01 M	3.02	−1.12	frust NMIN
0.01 M	3.20	−1.39	frust NMIN
0.01 M	3.51	−1.41	frust NMIN
0.01 M	4.02	−1.36	frust NMIN
0.01 M	4.21	−1.62	frust NMIN
0.01 M	4.53	−1.45	frust NMIN
0.01 M	5.01	−1.68	frust NMIN
0.01 M	5.27	−1.53	frust NMIN
0.01 M	11.97	−3.33	frust NMIN
0.01 M	10.82	−3.11	frust NMIN
0.01 M	8.64	−2.53	frust NMIN
0.01 M	6.36	−1.53	frust NMIN
0.01 M	11.82	−3.32	frust NMIN
0.01 M	11.49	−3.12	frust NMIN
0.01 M	10.24	−3.06	frust NMIN
0.01 M	8.97	−2.63	frust NMIN
0.01 M	2.00	−0.10	AMIN
0.01 M	2.16	−0.53	AMIN
0.01 M	2.45	−1.23	AMIN
0.01 M	2.99	−1.61	AMIN
0.01 M	3.16	−0.92	AMIN
0.01 M	3.46	−1.52	AMIN
0.01 M	4.12	−1.54	AMIN
0.01 M	4.27	−1.50	AMIN
0.01 M	4.72	−1.58	AMIN
0.01 M	5.57	−2.02	AMIN
0.01 M	11.95	−2.56	AMIN
0.01 M	11.03	−2.47	AMIN
0.01 M	9.99	−2.13	AMIN
0.01 M	7.49	−1.84	AMIN
0.01 M	6.78	−1.54	AMIN
0.01 M	6.18	−1.86	AMIN
0.01 M	8.96	−2.11	AMIN
0.01 M	7.91	−1.91	AMIN
0.1 M	1.51	−0.43	AMIN
0.1 M	2.01	−0.37	AMIN
0.1 M	2.23	−0.47	AMIN
0.1 M	2.54	−0.67	AMIN
0.1 M	3.04	−0.82	AMIN
0.1 M	3.20	−0.63	AMIN
0.1 M	4.09	−0.57	AMIN
0.1 M	4.33	−0.70	AMIN
0.1 M	4.60	−0.87	AMIN
0.1 M	5.27	−0.58	AMIN
0.1 M	5.65	−0.72	AMIN
0.1 M	12.54	−1.45	AMIN
0.1 M	9.40	−0.44	AMIN
0.1 M	9.40	−0.44	AMIN
0.1 M	7.65	−0.74	AMIN
0.1 M	6.73	−0.93	AMIN
0.1 M	10.27	−0.70	AMIN

Appendix 2. Summary of surface titration experiments performed in a modified limited residence time reactor.

I,M	Electrolyte	Conc. cell/L	Diatoms	pH	$[H^+]_S$, M
0.1	NaCl	2.3E+09	SC	10.51	−1.20E−03
0.1	NaCl	2.3E+09	SC	10.25	−7.07E−04
0.1	NaCl	2.3E+09	SC	10.18	−8.11E−04
0.1	NaCl	2.3E+09	SC	10.01	−5.93E−04
0.1	NaCl	2.3E+09	SC	9.98	−3.15E−04
0.1	NaCl	2.3E+09	SC	9.79	0.00E+00
0.1	NaCl	2.3E+09	SC	9.58	−1.61E−04
0.1	NaCl	2.3E+09	SC	9.44	−3.81E−04
0.1	NaCl	2.3E+09	SC	9.42	−8.82E−05
0.1	NaCl	2.3E+09	SC	9.41	5.66E−04
0.1	NaCl	2.3E+09	SC	9.29	−1.06E−04
0.1	NaCl	2.3E+09	SC	9.13	5.29E−04
0.1	NaCl	2.3E+09	SC	8.92	6.28E−04
0.1	NaCl	2.3E+09	SC	8.80	−1.42E−04
0.1	NaCl	2.3E+09	SC	8.70	9.31E−04
0.1	NaCl	2.3E+09	SC	8.56	1.16E−03
0.1	NaCl	2.3E+09	SC	8.04	2.64E−03
0.1	NaCl	2.3E+09	SC	7.25	2.48E−03
0.1	NaCl	2.3E+09	SC	6.83	3.88E−03
0.1	NaCl	2.3E+09	SC	6.73	4.08E−03
0.1	NaCl	2.3E+09	SC	6.72	4.08E−03
0.1	NaCl	2.3E+09	SC	6.27	5.58E−03
0.1	NaCl	2.3E+09	SC	5.82	7.05E−03
0.1	NaCl	2.3E+09	SC	5.68	7.00E−03
0.1	NaCl	2.3E+09	SC	5.02	8.43E−03
0.1	NaCl	2.3E+09	SC	4.90	8.40E−03
0.1	NaCl	2.3E+09	SC	4.11	9.15E−03
0.1	NaCl	2.3E+09	SC	3.09	8.93E−03
0.1	NaCl	2.3E+09	SC	2.82	9.55E−03
0.1	NaCl	2.3E+09	SC	2.60	9.94E−03
1	NaCl	2.3E+09	SC	10.38	−1.42E−03
1	NaCl	2.3E+09	SC	10.13	−1.10E−03
1	NaCl	2.3E+09	SC	9.90	−7.42E−04
1	NaCl	2.3E+09	SC	9.67	−4.64E−04
1	NaCl	2.3E+09	SC	9.54	−3.23E−04
1	NaCl	2.3E+09	SC	9.31	1.74E−04
1	NaCl	2.3E+09	SC	9.00	2.55E−04
1	NaCl	2.3E+09	SC	8.80	3.84E−04
1	NaCl	2.3E+09	SC	8.64	5.32E−04
1	NaCl	2.3E+09	SC	8.58	7.09E−04
1	NaCl	2.3E+09	SC	8.41	1.15E−03
1	NaCl	2.3E+09	SC	8.32	8.31E−04
1	NaCl	2.3E+09	SC	8.22	2.06E−03
1	NaCl	2.3E+09	SC	8.09	1.54E−03
1	NaCl	2.3E+09	SC	7.98	2.47E−03
1	NaCl	2.3E+09	SC	7.66	3.32E−03
1	NaCl	2.3E+09	SC	7.14	3.34E−03
1	NaCl	2.3E+09	SC	6.26	4.15E−03
1	NaCl	2.3E+09	SC	5.87	5.05E−03
1	NaCl	2.3E+09	SC	5.69	5.99E−03
1	NaCl	2.3E+09	SC	4.76	6.74E−03
1	NaCl	2.3E+09	SC	3.39	7.28E−03
1	NaCl	2.3E+09	SC	2.80	8.05E−03
0.001	NaCl	2.2E+09	TW	10.80	−4.60E−04
0.001	NaCl	2.2E+09	TW	10.42	−4.78E−04
0.001	NaCl	2.2E+09	TW	10.16	−3.16E−04
0.001	NaCl	2.2E+09	TW	9.82	−2.47E−04
0.001	NaCl	2.2E+09	TW	9.84	−2.37E−04
0.001	NaCl	2.2E+09	TW	9.55	−8.82E−05
0.001	NaCl	2.2E+09	TW	9.29	−9.04E−05
0.001	NaCl	2.2E+09	TW	8.93	−3.84E−05
0.001	NaCl	2.2E+09	TW	8.65	−1.11E−05
0.001	NaCl	2.2E+09	TW	8.43	2.50E−05
0.001	NaCl	2.2E+09	TW	7.26	4.48E−05
0.001	NaCl	2.2E+09	TW	6.57	4.67E−05
0.001	NaCl	2.2E+09	TW	6.01	1.04E−04
0.001	NaCl	2.2E+09	TW	5.77	1.71E−04

Appendix 2. (Continued)

I,M	Electrolyte	Conc. cell/L	Diatoms	pH	$[H^+]_S$, M
0.001	NaCl	2.2E+09	TW	5.38	1.96E−04
0.001	NaCl	2.2E+09	TW	5.27	2.20E−04
0.001	NaCl	2.2E+09	TW	4.28	3.86E−04
0.001	NaCl	2.2E+09	TW	4.06	5.10E−04
0.001	NaCl	2.2E+09	TW	3.81	6.19E−04
0.001	NaCl	2.2E+09	TW	3.52	6.71E−04
0.001	NaCl	2.2E+09	TW	3.31	6.49E−04
0.001	NaCl	2.2E+09	TW	3.28	6.39E−04
0.001	NaCl	2.2E+09	TW	3.11	7.22E−04
0.001	NaCl	2.2E+09	TW	2.97	7.69E−04
0.001	NaCl	2.2E+09	TW	2.76	7.36E−04
0.001	NaCl	2.2E+09	TW	2.67	7.96E−04
1	NaCl	2.2E+09	TW	11.12	−4.61E−04
1	NaCl	2.2E+09	TW	10.96	−4.58E−04
1	NaCl	2.2E+09	TW	10.86	−3.51E−04
1	NaCl	2.2E+09	TW	10.80	−3.48E−04
1	NaCl	2.2E+09	TW	10.48	−3.18E−04
1	NaCl	2.2E+09	TW	10.29	−2.24E−04
1	NaCl	2.2E+09	TW	9.96	−1.47E−04
1	NaCl	2.2E+09	TW	9.39	−6.28E−05
1	NaCl	2.2E+09	TW	8.41	−2.38E−05
1	NaCl	2.2E+09	TW	8.24	−2.00E−05
1	NaCl	2.2E+09	TW	7.96	3.74E−05
1	NaCl	2.2E+09	TW	7.54	2.92E−05
1	NaCl	2.2E+09	TW	7.25	5.06E−05
1	NaCl	2.2E+09	TW	6.76	6.36E−05
1	NaCl	2.2E+09	TW	6.30	7.42E−05
1	NaCl	2.2E+09	TW	5.75	9.70E−05
1	NaCl	2.2E+09	TW	5.56	2.26E−04
1	NaCl	2.2E+09	TW	4.80	2.70E−04
1	NaCl	2.2E+09	TW	4.10	3.63E−04
1	NaCl	2.2E+09	TW	3.90	4.86E−04
1	NaCl	2.2E+09	TW	3.83	4.35E−04
1	NaCl	2.2E+09	TW	3.79	4.21E−04
1	NaCl	2.2E+09	TW	3.42	4.83E−04
1	NaCl	2.2E+09	TW	3.44	6.26E−04
1	NaCl	2.2E+09	TW	3.28	6.17E−04
1	NaCl	2.2E+09	TW	3.46	7.52E−04
1	NaCl	2.2E+09	TW	2.96	7.67E−04
0.01	$NaNO_3$	1.5E+09	NMIN	11.50	−6.33E−04
0.01	$NaNO_3$	1.5E+09	NMIN	11.33	−5.67E−04
0.01	$NaNO_3$	1.5E+09	NMIN	10.80	−5.44E−04
0.01	$NaNO_3$	1.5E+09	NMIN	10.72	−4.63E−04
0.01	$NaNO_3$	1.5E+09	NMIN	10.43	−3.87E−04
0.01	$NaNO_3$	1.5E+09	NMIN	10.13	−3.51E−04
0.01	$NaNO_3$	1.5E+09	NMIN	10.04	−2.81E−04
0.01	$NaNO_3$	1.5E+09	NMIN	9.79	−2.27E−04
0.01	$NaNO_3$	1.5E+09	NMIN	9.29	−1.60E−04
0.01	$NaNO_3$	1.5E+09	NMIN	9.09	−1.59E−04
0.01	$NaNO_3$	1.5E+09	NMIN	9.09	−1.67E−04
0.01	$NaNO_3$	1.5E+09	NMIN	8.85	−7.73E−05
0.01	$NaNO_3$	1.5E+09	NMIN	8.57	−8.78E−05
0.01	$NaNO_3$	1.5E+09	NMIN	7.71	−9.81E−05
0.01	$NaNO_3$	1.5E+09	NMIN	7.68	−6.04E−05
0.01	$NaNO_3$	1.5E+09	NMIN	7.03	−2.99E−05
0.01	$NaNO_3$	1.5E+09	NMIN	6.50	6.79E−06
0.01	$NaNO_3$	1.5E+09	NMIN	6.43	3.21E−06
0.01	$NaNO_3$	1.5E+09	NMIN	6.33	1.77E−05
0.01	$NaNO_3$	1.5E+09	NMIN	6.21	3.09E−05
0.01	$NaNO_3$	1.5E+09	NMIN	5.91	5.06E−05
0.01	$NaNO_3$	1.5E+09	NMIN	5.64	7.01E−05
0.01	$NaNO_3$	1.5E+09	NMIN	5.30	8.49E−05
0.01	$NaNO_3$	1.5E+09	NMIN	4.80	9.27E−05
0.01	$NaNO_3$	1.5E+09	NMIN	4.80	9.61E−05
0.01	$NaNO_3$	1.5E+09	NMIN	4.31	1.58E−04
0.01	$NaNO_3$	1.5E+09	NMIN	3.87	1.90E−04
0.01	$NaNO_3$	1.5E+09	NMIN	3.56	2.51E−04
0.01	$NaNO_3$	1.5E+09	NMIN	3.34	2.57E−04

Appendix 2. (Continued)

I,M	Electrolyte	Conc. cell/L	Diatoms	pH	$[H^+]_S$, M
0.01	$NaNO_3$	1.5E+09	NMIN	3.21	2.81E−04
0.01	$NaNO_3$	1.5E+09	NMIN	3.09	2.78E−04
0.01	$NaNO_3$	1.5E+09	NMIN	2.94	3.37E−04
0.01	$NaNO_3$	1.5E+09	NMIN	2.82	3.80E−04
0.01	$NaNO_3$	1.5E+09	NMIN	2.47	4.56E−04
0.01	$NaNO_3$	1.5E+09	NMIN	2.28	5.52E−04
1	$NaNO_3$	1.5E+09	NMIN	10.61	−1.06E−03
1	$NaNO_3$	1.5E+09	NMIN	10.18	−7.01E−04
1	$NaNO_3$	1.5E+09	NMIN	9.66	−6.42E−04
1	$NaNO_3$	1.5E+09	NMIN	9.06	−4.53E−04
1	$NaNO_3$	1.5E+09	NMIN	9.00	−5.63E−04
1	$NaNO_3$	1.5E+09	NMIN	8.67	−3.84E−04
1	$NaNO_3$	1.5E+09	NMIN	8.67	−3.84E−04
1	$NaNO_3$	1.5E+09	NMIN	8.47	−2.95E−04
1	$NaNO_3$	1.5E+09	NMIN	7.88	−2.12E−04
1	$NaNO_3$	1.5E+09	NMIN	7.72	−2.16E−04
1	$NaNO_3$	1.5E+09	NMIN	7.64	−1.78E−04
1	$NaNO_3$	1.5E+09	NMIN	7.24	−1.26E−04
1	$NaNO_3$	1.5E+09	NMIN	7.16	−1.28E−04
1	$NaNO_3$	1.5E+09	NMIN	6.93	−9.24E−05
1	$NaNO_3$	1.5E+09	NMIN	6.75	−6.42E−05
1	$NaNO_3$	1.5E+09	NMIN	6.45	−3.24E−05
1	$NaNO_3$	1.5E+09	NMIN	6.22	−1.36E−05
1	$NaNO_3$	1.5E+09	NMIN	5.64	3.52E−06
1	$NaNO_3$	1.5E+09	NMIN	5.40	9.78E−06
1	$NaNO_3$	1.5E+09	NMIN	5.23	2.03E−05
1	$NaNO_3$	1.5E+09	NMIN	4.90	4.27E−05
1	$NaNO_3$	1.5E+09	NMIN	4.54	8.99E−05
1	$NaNO_3$	1.5E+09	NMIN	4.20	1.09E−04
1	$NaNO_3$	1.5E+09	NMIN	3.97	1.68E−04
1	$NaNO_3$	1.5E+09	NMIN	3.68	1.75E−04
1	$NaNO_3$	1.5E+09	NMIN	3.41	2.13E−04
1	$NaNO_3$	1.5E+09	NMIN	3.01	2.40E−04
0.01	NaCl	2.1E+09	AMIN	11.24	−2.67E−04
0.01	NaCl	2.1E+09	AMIN	11.14	−2.65E−04
0.01	NaCl	2.1E+09	AMIN	10.95	−2.57E−04
0.01	NaCl	2.1E+09	AMIN	10.63	−2.11E−04
0.01	NaCl	2.1E+09	AMIN	10.50	−2.03E−04
0.01	NaCl	2.1E+09	AMIN	9.49	−1.26E−04
0.01	NaCl	2.1E+09	AMIN	9.22	−1.12E−04
0.01	NaCl	2.1E+09	AMIN	8.89	−1.01E−04
0.01	NaCl	2.1E+09	AMIN	8.55	−9.46E−05
0.01	NaCl	2.1E+09	AMIN	8.30	−9.80E−05
0.01	NaCl	2.1E+09	AMIN	7.90	−8.35E−05
0.01	NaCl	2.1E+09	AMIN	7.08	−5.03E−05
0.01	NaCl	2.1E+09	AMIN	6.92	−2.96E−05
0.01	NaCl	2.1E+09	AMIN	6.84	−3.29E−05
0.01	NaCl	2.1E+09	AMIN	6.73	−1.44E−05
0.01	NaCl	2.1E+09	AMIN	6.34	−2.79E−07
0.01	NaCl	2.1E+09	AMIN	5.83	2.00E−05
0.01	NaCl	2.1E+09	AMIN	5.70	2.85E−05
0.01	NaCl	2.1E+09	AMIN	5.49	2.85E−05
0.01	NaCl	2.1E+09	AMIN	5.10	3.37E−05
0.01	NaCl	2.1E+09	AMIN	4.79	3.22E−05
0.01	NaCl	2.1E+09	AMIN	4.56	4.05E−05
0.01	NaCl	2.1E+09	AMIN	4.39	4.50E−05
0.01	NaCl	2.1E+09	AMIN	4.16	5.66E−05
0.01	NaCl	2.1E+09	AMIN	4.01	6.82E−05
0.01	NaCl	2.1E+09	AMIN	3.75	8.15E−05
0.01	NaCl	2.1E+09	AMIN	3.57	8.50E−05
0.01	NaCl	2.1E+09	AMIN	3.45	8.72E−05
0.01	NaCl	2.1E+09	AMIN	3.27	1.01E−04
0.01	NaCl	2.1E+09	AMIN	3.21	1.03E−04
0.01	NaCl	2.1E+09	AMIN	3.09	1.09E−04
0.01	NaCl	2.1E+09	AMIN	3.01	1.22E−04
0.01	NaCl	2.1E+09	AMIN	2.82	1.31E−04
0.1	NaCl	2.1E+09	AMIN	11.04	−3.15E−04
0.1	NaCl	2.1E+09	AMIN	10.74	−3.26E−04

Appendix 2. (Continued)

I,M	Electrolyte	Conc. cell/L	Diatoms	pH	$[H^+]_S$, M
0.1	NaCl	2.1E+09	AMIN	10.54	−2.71E−04
0.1	NaCl	2.1E+09	AMIN	10.37	−2.64E−04
0.1	NaCl	2.1E+09	AMIN	10.00	−2.24E−04
0.1	NaCl	2.1E+09	AMIN	9.09	−1.57E−04
0.1	NaCl	2.1E+09	AMIN	9.06	−1.59E−04
0.1	NaCl	2.1E+09	AMIN	8.47	−1.30E−04
0.1	NaCl	2.1E+09	AMIN	8.28	−1.11E−04
0.1	NaCl	2.1E+09	AMIN	8.03	−9.18E−05
0.1	NaCl	2.1E+09	AMIN	7.65	−7.49E−05
0.1	NaCl	2.1E+09	AMIN	7.32	−5.74E−05
0.1	NaCl	2.1E+09	AMIN	7.10	−3.80E−05
0.1	NaCl	2.1E+09	AMIN	6.97	−2.89E−05
0.1	NaCl	2.1E+09	AMIN	6.73	−2.39E−05
0.1	NaCl	2.1E+09	AMIN	6.16	2.13E−05
0.1	NaCl	2.1E+09	AMIN	5.93	1.04E−05
0.1	NaCl	2.1E+09	AMIN	5.51	1.80E−05
0.1	NaCl	2.1E+09	AMIN	5.17	2.26E−05
0.1	NaCl	2.1E+09	AMIN	4.89	3.01E−05
0.1	NaCl	2.1E+09	AMIN	4.64	3.97E−05
0.1	NaCl	2.1E+09	AMIN	4.57	5.93E−05
0.1	NaCl	2.1E+09	AMIN	4.39	7.03E−05
0.1	NaCl	2.1E+09	AMIN	4.19	7.40E−05
0.1	NaCl	2.1E+09	AMIN	4.06	1.01E−04
0.1	NaCl	2.1E+09	AMIN	3.78	1.42E−04
0.1	NaCl	2.1E+09	AMIN	3.54	1.58E−04
0.1	NaCl	2.1E+09	AMIN	3.30	1.94E−04
0.1	NaCl	2.1E+09	AMIN	3.13	2.15E−04
0.1	NaCl	2.1E+09	AMIN	3.01	2.45E−04
0.1	NaCl	8.9E+09	AMIN	11.03	−1.21E−03
0.1	NaCl	8.9E+09	AMIN	10.76	−1.17E−03
0.1	NaCl	8.9E+09	AMIN	10.59	−1.12E−03
0.1	NaCl	8.9E+09	AMIN	10.34	−1.03E−03
0.1	NaCl	8.9E+09	AMIN	10.05	−9.03E−04
0.1	NaCl	8.9E+09	AMIN	9.45	−8.15E−04
0.1	NaCl	8.9E+09	AMIN	9.01	−6.22E−04
0.1	NaCl	8.9E+09	AMIN	8.81	−5.12E−04
0.1	NaCl	8.9E+09	AMIN	8.32	−4.04E−04
0.1	NaCl	8.9E+09	AMIN	7.93	−2.80E−04
0.1	NaCl	8.9E+09	AMIN	7.37	−1.56E−04
0.1	NaCl	8.9E+09	AMIN	7.36	−1.51E−04
0.1	NaCl	8.9E+09	AMIN	7.14	−1.10E−04
0.1	NaCl	8.9E+09	AMIN	6.98	−6.91E−05
0.1	NaCl	8.9E+09	AMIN	6.74	−3.71E−05
0.1	NaCl	8.9E+09	AMIN	6.55	1.89E−05
0.1	NaCl	8.9E+09	AMIN	6.45	3.31E−05
0.1	NaCl	8.9E+09	AMIN	6.31	4.18E−05
0.1	NaCl	8.9E+09	AMIN	6.11	4.19E−05
0.1	NaCl	8.9E+09	AMIN	5.95	9.55E−05
0.1	NaCl	8.9E+09	AMIN	5.55	1.77E−04
0.1	NaCl	8.9E+09	AMIN	4.58	3.83E−04
0.1	NaCl	8.9E+09	AMIN	4.08	5.53E−04
0.1	NaCl	8.9E+09	AMIN	3.65	6.44E−04
0.1	NaCl	8.9E+09	AMIN	3.39	7.17E−04
0.1	NaCl	8.9E+09	AMIN	3.18	8.40E−04
0.1	NaCl	8.9E+09	AMIN	3.00	8.81E−04
0.1	NaCl	8.9E+09	AMIN	2.84	9.31E−04